arXiv:2003.08405v1 [hep-th] 18 Mar 2020

Exploring Hamiltonian Truncation in d = 2 + 1

Joan Elias Miró[a,b], **Edward Hardy**[c]

[a] ICTP, Strada Costiera 11, 34135, Trieste, Italy
[b] CERN, Theoretical Physics Dep., 1211 Geneva 23, Switzerland
[c] University of Liverpool, Dept. of Mathematical Sciences, Liverpool L69 7ZL, United Kingdom

Abstract

We initiate the application of Hamiltonian Truncation methods to solve strongly coupled QFTs in $d = 2 + 1$. By analysing perturbation theory with a Hamiltonian Truncation regulator, we pinpoint the challenges of such an approach and propose a way that these can be addressed. This enables us to formulate Hamiltonian Truncation theory for ϕ^4 in $d = 2 + 1$, and to study its spectrum at weak and strong coupling. The results obtained agree well with the predictions of a weak/strong self-duality possessed by the theory. The ϕ^4 interaction is a strongly relevant UV divergent perturbation, and represents a case study of a more general scenario. Thus, the approach developed should be applicable to many other QFTs of interest.

Contents

1 Introduction . . . 3
2 Hamiltonian Truncation . . . 5
2.1 Definitions . . . 5
2.2 The approach . . . 5
3 Perturbation theory . . . 7
3.1 Examples . . . 8
3.2 Rules . . . 10
4 ϕ^2 test . . . 11
4.1 Analytic solution . . . 11
4.2 Perturbative solution . . . 11
4.3 Hamiltonian Truncation solution . . . 15
5 Hamiltonian Truncation for a UV divergent perturbation . . . 16
5.1 Problems with naive perturbation theory . . . 18
5.2 The general case . . . 19
5.3 Patching up perturbation theory with E_T regularisation . . . 25
5.4 Hamiltonian Truncation formulation . . . 28
6 Results from truncations . . . 29
7 Crosscheck through a weak/strong self-duality . . . 32
7.1 Theory . . . 32
7.2 Numerical results . . . 34
8 Summary and outlook . . . 37

Appendices:

A Basis of states on a square torus . . . 39
B Perturbation theory . . . 40
B.1 Principal equations . . . 40
B.2 Cancelation of disconnected two-point bubbles . . . 41
C Calculation of counter-terms . . . 42
D Perturbative mass . . . 43
E Algorithmic implementation . . . 44
F Finite mismatch pieces . . . 45
F.1 Sources of finite regulator dependence . . . 46
F.2 Finite pieces and the weak/strong self-duality . . . 47
G Monte Carlo integration of low order diagrams . . . 48

1 Introduction

There is currently no known universal and efficient method to derive the phenomenological implications of strongly coupled Quantum Field Theories (QFTs). Thus any new strategy to understand the strongly coupled regime merits scrutiny. In this paper we analyse one such approach: the Hamiltonian Truncation (HT) method.

The basic idea behind HT is quite transparent, consisting of a generalisation of the Rayleigh-Ritz method of Quantum Mechanics to QFT: Consider a theory whose Hamiltonian can be decomposed as $H = H_0 + V$, where H_0 denotes a solvable Hamiltonian [1] – $H_0|E_i\rangle = E_i|E_i\rangle$ – and V denotes a perturbation. Then, HT proceeds by truncating the Hamiltonian H into a large finite matrix H_{ij} with $E_i \leqslant E_T$, and diagonalising it numerically. There is a systematic error due to the truncation energy E_T, however in many instances the spectrum of the full theory can be recovered from results obtained at finite E_T by performing precise extrapolations $E_T \to \infty$. [2]

Although conceptually simple, the strength of the HT idea is that it can be used to tackle strongly coupled QFTs. Indeed, it has been applied very successfully in $d = 2$ spacetime dimensions. There are various incarnations of the method differing in the quantisation frame and the choices of basis and H_0. One important version is the Truncated Conformal Space Approach (TCSA) introduced in [1, 2], which sparked numerous further studies. In TCSA the Hamiltonian H_0 is that of a solvable two dimensional CFT. [3] More recently, a closely related version, coined Conformal Truncation, exploits light-cone quantisation to truncate the wave-functions at infinite volume [3–7]. Another guise of HT uses a massive Fock-Space basis to truncate the Hamiltonian. Early work on this direction was done in [8]. Since then, the method has been developed in [9–12] and results with a precision that is competitive with other up to date techniques have been obtained [13].

The literature on HT in $d = 2$ is by now extensive, with a plethora of fascinating results for strongly coupled QFTs. For example, HT has allowed strongly coupled real time dynamics, and strongly coupled perturbations of interacting fixed points, to be studied. We refer the reader to [14] for a review where further references may also be found.

Despite this success in $d = 2$, it has remained an unsolved challenge to apply the ideas of HT to $d \geqslant 3$ strongly coupled QFTs. The main obstacle is the appearance of UV divergences that require regularisation. In particular, divergences appear in many QFTs that we care about for $d \geqslant 3$, when the QFT is formulated by perturbing a solvable theory by a relevant operator, $H_0 \to H_0 + V$. The E_T cutoff is a natural regulator for the divergences. But then, what are the counter-terms required to formulate HT? And, is a covariant Lorentz spectrum recovered as the E_T regulator is removed? In this paper we will address these, and other, key open questions.

We will be pragmatic and approach these problems in a particular instance of HT, using the massive Fock-Space basis. We will study the ϕ^4_3 theory, namely we will perturb the free massive theory by the operator $V = g\int \phi^4$ in $d = 2 + 1$. This is a relevant operator, in the RG sense.

[1] A free-theory or an interacting integrable theory, be it a solvable CFT or and integrable massive QFT.

[2] We will formulate HT more precisely in section 2.

[3] More precisely, the CFT is placed on the cylinder $\mathbb{R} \times S^1_R$ of radius R. Then, due to the state-operator map, H_0 is the dilatation operator and the role of E_T is played by the dimension of a heavy operator $E_T \sim \Delta_{\max}/R$.

Thus, very naively, we may expect that the spectrum will converge in a power-like manner g/E_T as E_T is increased. However, the ϕ_3^4 theory has a linear UV divergence associated to the vacuum and a logarithmic UV divergence associated to the mass. Thus, it will act as a prototype case study, capturing the key features of a far more general class of theories. In particular, many of the techniques that we will develop should be useful for formulating HT in any dimension for theories in which V is a strongly relevant perturbation.

We will study the theory at finite volume. This allows us to focus on the UV conundrums without having to deal with other problems associated to the large volume dynamics, such as the orthogonality catastrophe recently analysed in [15]. It would be very interesting to carry out a separate investigation of the infinite volume limit in the future.

There have been various interesting works prior to us in $d > 2$ that we would like to highlight. In [16] the TCSA method was developed at $2 < d \leqslant 2.5$ spacetime dimensions. In this range of d the UV divergences of the ϕ_d^4 theory are absent. Then, ref. [17] investigated, among other things, the allowed counter-terms at second order in perturbation theory in TCSA for general d. [4] In the Conformal Truncation line of development, ref. [5] studied ϕ_3^4 at weak coupling, and the $(\vec{\phi}.\vec{\phi})^2$ perturbation for large vector size N. Meanwhile ref. [18] laid down formulas to efficiently compute the matrix elements of ϕ_3^4 in the Conformal Truncation approach. Finally, other recent work has been done in [19]. There, the main results for $d = 3$ [on a S_3 manifold] are restricted to ϕ^2 and $i\phi^3$ perturbations, where the UV divergences are either absent or only logarithmic.

First, we review the basics of HT and Hamiltonian perturbation theory in section 2 and 3, respectively. Then, our strategy is as follows. The results of Hamiltonian Truncation at weak coupling must match those of perturbation theory. Therefore, we begin our main investigation by analysing perturbation theory regulated with an E_T cutoff. In section 4 we analyse the ϕ_3^2 perturbation from three perspectives: the exact solution, the Hamiltonian perturbation theory solution, and HT. Then, in section 5 we study the ϕ_3^4 theory. Although in this case we do not know the exact solution, we carry out an analogous perturbation theory analysis. The E_T cutoff is a rather unusual regulator and various surprises lie ahead. For instance, disconnected vacuum diagrams cancel in an intricate manner in Hamiltonian Perturbation theory; and we find that such cancelation is spoiled with the ET regularisation, introducing new UV divergences. We manage to precisely delineate all such challenges and we offer a solution in section 5.

After understanding perturbation theory, we uplift our formalism into Hamiltonian Truncation. In section 6 we start our numerical explorations. First we implement HT and find agreement with perturbation theory. Having matched perturbation theory and seen that extrapolations to large E_T are feasible, we increase the coupling in section 7. There we perform a crosscheck of the strong coupling spectrum by making use of a strong/weak self-duality that the theory possesses. Finally, we conclude and discuss some of the many interesting possible directions for future work in section 8.

[4] As we will show below many interesting effects start at fourth and higher order.

2 Hamiltonian Truncation

We begin our study of Hamiltonian Truncation in higher dimensions focusing on the $(\phi^2)_3$ and $(\phi^4)_3$ perturbations at finite volume. In this section we review the basics of HT and set our conventions.

2.1 Definitions

The theory that we study is defined by deforming the free massive theory by a strongly relevant perturbation, $(\phi^4)_3$. The free theory is quantized on a flat torus space of size $L \times L$, and the time direction is left uncompact $t \in \mathbb{R}$. We impose periodic boundary conditions on the operator $\phi(t, x, y) = \phi(t, x, y + nL) = \phi(t, x + nL, y)$ for $n \in \mathbb{Z}$. Since the space directions are compact the spectrum of the free theory is discrete and free of IR divergences. In canonical quantization ϕ can be expanded in terms of creation and annihilation operators as

$$\phi(0, x) = \sum_k a_k e^{-ik\cdot\mathbf{x}} / \sqrt{2L^2\omega_k} + h.c. \tag{2.1}$$

where $k = (k_1, k_2)$, $k_i = 2\pi n_i/L$, $n_i \in \mathbb{Z}$, $\omega_k = (k_1^2 + k_2^2 + m^2)^{1/2}$ and $a^\dagger$, a satisfy the algebra of creation/annihilation operators $[a_k, a^\dagger_{k'}] = \delta_{k,k'}\,, \quad [a_k, a_{k'}] = 0$. The free Hamiltonian is $H_0 = \sum_{\mathbf{k}} \omega_k a^\dagger_k a_k$ and it is diagonalized by the H_0 eigenbasis basis $|E_i\rangle = \frac{a^{\dagger n_N}_{k_N}}{\sqrt{n_N!}} \cdots \frac{a^{\dagger n_2}_{k_2}}{\sqrt{n_2!}} \frac{a^{\dagger n_1}_{k_1}}{\sqrt{n_1!}} |0\rangle$ with eigenvalues $E_i = \sum_{s=1}^N n_s \sqrt{k_s^2 + m^2}$. [5] The free vacuum is defined by $H_0 |0\rangle = 0$.

The interacting Hamiltonian is

$$H(E_T) = H_0 + V \quad \text{with} \quad V = g_2 V_2 + g_4 V_4 + C(E_T) \tag{2.2}$$

where

$$V_n = \frac{1}{n!} \int_{-L/2}^{+L/2} d^2x \; :\phi^n(x): \;, \tag{2.3}$$

and $:\phi^n(x):$ indicates normal ordering, i.e. annihilation operators are placed to the right of creation operators. [6] The operator C in (2.2) is a counter-term that must take a somewhat unusual form and will be explained in the sections below. For future use we define $O_{ij} \equiv \langle E_i | O | E_j \rangle$ and $g_4 \equiv g$.

2.2 The approach

The Hamiltonian defined in section 2.1 acts in the Hilbert space $\mathcal{H}$ spanned by the free states $|E_i\rangle$. In the Hamiltonian Truncation approach, we study the theory by considering only states $E_i \leqslant E_T$,

[5] In (2.1) k_i is obviously a two-dimensional vector [instead of components of k, below (2.1)]. From here on any subscripted momenta is a label for a two-dimensional vector.

[6] Normal ordering in finite volume differs from the normal ordering in infinite volume. The difference is a scheme choice and it can be accounted for by finite counterterms that are exponentially small in the large volume limit [9].

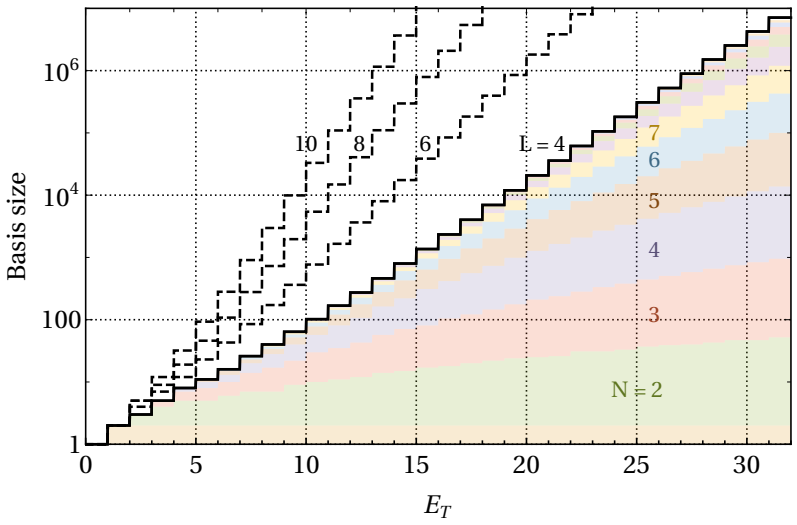


Figure 1: The size of the Fock space basis as a function of E_T for $m = 1$ and different box sizes L. For $L = 4$ the contributions from basis elements with different occupation numbers N is shown.

with the counter-terms in (2.2) evaluated at E_T. In this case the Hamiltonian (2.2) can be viewed as the finite dimensional matrix

$$H_{ij} = \langle E_i | \, H \, | E_j \rangle \ . \tag{2.4}$$

The spectrum of H can then be obtained by applying a numerical routine to obtain the lowest few eigenvalues of H_{ij}. Similarly to Hamiltonian Perturbation theory, the actual theory that we are interested in is recovered by removing the regulator, i.e. taking the limit $E_T \to \infty$. In practice this is done by considering a series of Hamiltonians $H(E_T^{(i)})$ with $E_T^{(0)} < E_T^{(1)} < \cdots < E_T^{(n)}$ such that $E_T^{(n)} \gg m$, and extrapolating the eigenvalues to infinite E_T.

The symmetry transformations of the theory (2.2) can be used to simplify the task of obtaining the eigenvalues of H. These transformations are the field parity $\mathbb{Z}_2$ ($\phi(x) \to -\phi(x)$), the momentum, and the finite subgroup of O(2) that corresponds to the symmetry group of a flat torus [further details may be found in appendix A]. The matrix (2.4) can therefore be diagonalised separately in the different selection sectors. Throughout this paper we focus on states with zero total momenta, and we diagonalise the $\mathbb{Z}_2 = \pm$ sectors separately. We have verified that the lowest lying states are in the singlet sector of the square torus transformations, as expected from perturbation theory. Therefore we restrict to this sector in what follows.

A basis of the Hilbert space up to a given cutoff E_T can be straightforwardly constructed in a computer program. Then the Hamiltonian can be calculated, although some care is required in the algorithm to enable large basis sizes to be reached. The lowest lying eigenvalues can be obtained using standard algorithms, for example based on the Lanczos method. Further details on our numerical approach can be found in appendix E.

In Figure 1 we plot the size of the singlet sector of the basis for a theory with $m = 1$ as a function of the cutoff energy for E_T [including both field parity sectors]. Using moderate computational resources we are able to obtain eigenvalues for bases of size up to $\sim 10^7$. We see that our numerical reach corresponds to $E_T/m \sim 32$ for a box of length $L = 4/m$, which will turn out to be sufficient

to perform reasonable extrapolations $E_T \to \infty$.

3 Perturbation theory

At weak coupling, the spectrum of the truncated Hamiltonian can be computed using Hamiltonian Perturbation Theory (HPT), a.k.a. Old Fashioned Perturbation Theory. Throughout the paper we will make extensive use of HPT. Since HPT is somewhat in disuse, in this section we provide a basic review and set up the notation – the reader familiar with such material may safely skip this section.

In perturbation theory we compute the ith energy level in a truncated power series of the interaction strength $\mathcal{E}_i = \sum_n \mathcal{E}_i^{(n)}$. The general structure of the corrections $\mathcal{E}_i^{(n)}$ is always the same, namely, the nth order correction is given by

$$\mathcal{E}_i^{(n)} = \langle E_i | \hat{V}([E_i - H_0]^{-1}\hat{V})^{n-1} | E_i \rangle - \text{subtraction terms}\,, \tag{3.1}$$

where we have defined $\hat{V} = PVP$, and P is the projector $P = \mathbb{1} - |E_i\rangle\langle E_i|$. The role of the *subtraction terms* will be clarified in the sections below, and they will turn out to be crucial for our work. For instance, the first terms of perturbation theory for the energy levels are given by

$$\begin{aligned}\mathcal{E}_i &= \underbrace{V_{ii}}_{\mathcal{E}_i^{(1)}} + \underbrace{V_{ik}\frac{1}{E_{ik}}V_{ki}}_{\mathcal{E}_1^{(2)}} + \underbrace{V_{ik}\frac{1}{E_{ik}}V_{kk'}\frac{1}{E_{ik'}}V_{k'i} - V_{ii}\,V_{ik}\frac{1}{E_{ik}^2}V_{ki}}_{\mathcal{E}_0^{(3)}} \\ &+ \underbrace{\frac{V_{ik}V_{kk'}V_{k'k''}V_{k''i}}{E_{ik}E_{ik'}E_{ik''}} - \mathcal{E}_i^{(2)}\,\frac{V_{ik}V_{ki}}{E_{ik}^2} - 2V_{ii}\,\frac{V_{ik}V_{kk'}V_{k'i}}{E_{ik}^2E_{ik'}} - V_{ii}^2\,\frac{V_{ik}V_{ki}}{E_{ik}^3}}_{\mathcal{E}_0^{(4)}} + O(V^5)\,,\end{aligned} \tag{3.2}$$

where $E_{ij} = E_i - E_j$, and a sum over intermediate states $k, k', k'' \neq i$ is implicit. See appendix B.1 for a derivation of (3.2).

To calculate (3.2), we can proceed by evaluating the expressions $\langle E_i | F_n(z) | E_i \rangle = \langle E_i | V([z - H_0]^{-1}V)^{n-1} | E_i \rangle$. These can be conveniently written as

$$F_n(z + E_i) = (-i)^{n-1}\int_0^\infty dt_1 \cdots dt_{n-1}\; e^{iz(t_1+\cdots t_{n-1})}\, V(T_{n-1})\, V(T_{n-2}) \cdots V(0)\;, \tag{3.3}$$

where $T_k = \sum_{i=1}^{i=k} t_i$, $V(t) = e^{iH_0 t}Ve^{-iH_0 t}$. [7] From (3.3) it is easy to extract (3.2). Eq. (3.3) is time ordered in the whole integration domain and thus we can apply Wick's theorem. For concreteness let us take $V = g_k\phi^k/k!$, generalisations are straightforward. Applying Wick's theorem to the product $V(T_{n-1})\, V(T_{n-2}) \cdots V(0)$ we get

$$\frac{g_k^n}{k!^n}\int_{L/2}^{L/2}\prod_{i=0}^{n-1} d^2y_i\; s^k_{\{n_{a,b}\}}\prod_{a=1}^{n-1}\prod_{b=0}^{a-1} D_{ab}^{n_{a,b}}\; :\phi_{Y_{n-1},T_{n-1}}^{k-\Sigma_{s\neq n-1}n_{n-1,s}}\phi_{Y_{n-2},T_{n-2}}^{k-\Sigma_{s\neq n-2}n_{n-2,s}}\cdots\phi_{Y_0,T_0}^{k-\Sigma_{s\neq 0}n_{0,s}}:\,, \tag{3.4}$$

[7] Generically we will need $F(z_1, z_2, \ldots, z_n) = V\prod_{i=1}^n (z_i - H_0)^{-1}V$ and its derivatives, which involves a straightforward generalisation. Note also that the integrals in (3.3) converge for $\mathrm{Im} z > 0$, and for other values of z analytic continuation is understood.

where $\phi_{x,t} \equiv \phi(x,t)$. $D_{ij} \equiv D(x_i^\mu - x_j^\mu)$ is the propagator joining the points $(\vec{Y}_i, T_i)$ and $(\vec{Y}_j, T_j)$, where $\vec{Y}_i = \vec{y}_0 + \sum_{p=1}^{i} \vec{y}_p$, given by

$$\theta(t) D(\vec{z}, t) = \sum_{\vec{k}} \frac{1}{2L^2 \omega_{\vec{k}}} e^{-i\omega_{\vec{k}} t + i\vec{k}\cdot\vec{z}} . \tag{3.5}$$

The tensor $n_{a,b} = n_{b,a}$ is symmetric and takes indices in the numbered vertices $V(T_a)$. Thus, if we have a number $n_{1,2}$ of propagators connecting the 1 and 2 vertices, these same number of fields is subtracted from the vertices $\phi^k_{Y_1,T_1}$ and $\phi^k_{Y_2,T_2}$. Finally the combinatoric factor $s_{\{n_{a,b}\}}$ is given by

$$s^k_{\{n_{a,b}\}} = \frac{k!^n}{\prod_{j=0}^{n-1} (k - \Sigma_{s\neq j} n_{j,s})!} \frac{1}{\prod_{a=1}^{n-1} \prod_{b=0}^{a-1} n_{a,b}!} . \tag{3.6}$$

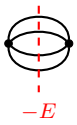
Upon plugging the field mode expansion (2.1) and the propagators (3.5) into equations (3.3) and (3.4), we can perform the straightforward integrals over the exponentials and we are left with a sum over the momentum modes. Since the index structure in Formula (3.4) is somewhat involved, let us give a couple of examples.

3.1 Examples

For instance for $k = 4$, the $O(g^2)$ correction to the vacuum is computed as follows

$$V_{0k} E_k^{-1} V_{k0} = \frac{g^2 L^2 s_4^4}{4!^2} \int_0^\infty dt_1 e^{izt_1} \int_{-L/2}^{L/2} d^2 y_1 D^4(\vec{y}_1, t_1) , \tag{3.7}$$

with $s_p^k = k!^2/(k-p)!^2/p!$. Upon performing the straightforward integrals of the previous expression we get



$$= \frac{(gL)^2}{24} \sum_{\vec{k}_i} \underbrace{\frac{L^2 \delta_{\vec{k}_1+\vec{k}_2+\vec{k}_3+\vec{k}_4}}{-(\omega_{\vec{k}_1} + \omega_{\vec{k}_2} + \omega_{\vec{k}_2} + \omega_{\vec{k}_4})}}_{-E} , \tag{3.8}$$

where we have introduced the Feynman diagrammatic notation that we review later. Here and in many examples below, it will be convenient to write the sum over the intermediate states in (3.8) in terms of the relativistic phase-space. At $d = 2 + 1$, the finite volume phase space is given by

$$\Phi_n(P^\mu) = \sum_{k's} \frac{1}{\prod_j 2L^2 \omega_{\vec{k}_j}} L^2 \delta_{\Sigma_i \vec{k}_i, \vec{P}} (2\pi) \delta(\Sigma_i \omega_{\vec{k}_i} - E) , \tag{3.9}$$

where $P^\mu = (E, \vec{P})$. Its infinite volume limit can be computed in $d = 2 + 1$ and it is given by

$$\Phi_n(\sqrt{s}) \overset{L\to\infty}{\longrightarrow} \int_{-\infty}^{\infty} \prod_{s=1}^{n} \frac{d^2 k_s}{(2\pi)^2 2\omega_{\vec{k}_s}} \delta^{(3)}(\Sigma_{i=1}^n k_i^\mu - P^\mu) = \frac{\pi^{2-n} 4^{1-n}}{(n-2)!} \frac{(\sqrt{s} - n\sqrt{m^2})^{n-2}}{\sqrt{s}} , \tag{3.10}$$

where $s = P_\mu^2$, see for instance [20]. Thanks to the closed form expression in (3.10) we will be able to analytically evaluate many HPT diagrams with a large number of loops. Now, upon inserting $1 = \int_{4m}^{E_T} dE \delta(E - \Sigma_i \omega_{k_i})$ in (3.8) we get

$$(3.8) = -\frac{(gL)^2}{24} \int_{4m}^{E_T} \frac{dE}{2\pi} \frac{\Phi_4(E)}{E} , \tag{3.11}$$

where we have introduced a regulator by cutting the maximal energy of the intermediate state $E_k \leqslant E_T$. More generally, regulating the theory with an energy cutoff E_T – so that all Fock space states have H_0-energies $E_i \leqslant E_T$ – corresponds to requiring that the energy of the states between the vertices in (3.3) is $E_i \leqslant E_T$. This can be easily implemented in the HPT diagrams by imposing that each of the energy propagators is bounded from below by $1/E_T$. [8] The value of (3.11) in the infinite volume limit is straightforwardly computed using (3.10).

As a second example, consider a mass perturbation, i.e. $k = 2$. Then (3.3)-(3.4) for $n = 2$ gives

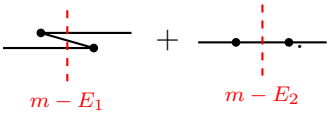
$$-\frac{ig^2}{2!^2}\int_0^\infty dt \int_{-L/2}^{+L/2} d^2x d^2z \sum_{p=0}^{2} s_p^2 D_F^p(\vec{z},t) \; : \phi^{2-p}_{(\vec{x}+\vec{z},t/2)}\phi^{2-p}_{(\vec{x},-t/2)} : \tag{3.12}$$

For concreteness let us compute the $p = 1$ Wick's contraction and take the expectation value with the one particle state at rest $|m\rangle$, i.e.

$$-i\frac{g_2^2 L^2}{2}\int_0^\infty dt\, e^{it(\epsilon-m)} \int_{-L/2}^{+L/2} d^2z D_{(\vec{z},t)} \langle m| : \phi(\vec{z},t)\phi(0,0) : |m\rangle \tag{3.13}$$

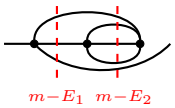
where $\epsilon \to i0_+$. Carrying out all the integrals of the previous expression we get

$$(3.13) = \frac{g_2^2}{4m^2}\underbrace{\frac{1}{m-3m}}_{m-E_1} + \frac{g_2^2}{4m^2}\underbrace{\frac{1}{m-m}}_{m-E_2} + \epsilon = \tag{3.14}$$

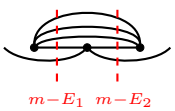


If this was the calculation of $V_{1k}E_{1k}^{-1}V_{k1}$ in (3.2), the second diagram would not contribute and needs to be discarded because the energy of the state between the two vertices is $E_k = 1$. This is a particular instance of a general rule: when computing (3.2) through the correlation functions (3.4) we need to discard those contributions in which the state being propagated between two consecutive vertices is equal to E_i. Note that there are two possible vertex orderings in (3.14) giving rise to two different expressions.

Indeed the order of the vertices matters because the integrand (3.3) is time-ordered in the whole integration domain, thus diagrams differing by the vertex ordering give rise to different expressions. A more dramatic instance occurs in the following corrections to the 1-particle state



$$= \frac{g^3}{6m}\sum \underbrace{\frac{L^2\delta_{q+p,0}}{m-(\omega_p+\omega_q+m)}}_{m-E_1}\underbrace{\frac{L^2\delta_{p+k_1+k_2+k_3,0}}{m-(\omega_p+\omega_{k_1}+\omega_{k_2}+\omega_{k_3}+m)}}_{m-E_2}, \tag{3.15}$$



$$= \frac{g^3}{6m}\sum \underbrace{\frac{L^2\delta_{k_1+k_2+k_3+p,0}}{m-(\omega_{k_1}+\omega_{k_2}+\omega_{k_3}+\omega_p+m)}}_{m-E_1}\underbrace{\frac{L^2\delta_{k_1+k_2+k_3+q,0}}{m-(\omega_{k_1}+\omega_{k_2}+\omega_{k_3}+\omega_q+m)}}_{m-E_2}, \tag{3.16}$$

where for simplicity we defined $\sum \equiv \sum_{\substack{\text{momenta}\\ \text{s.t. } E_i\leqslant E_T}} \frac{1}{\prod_i 2\omega_i L^2}$ i.e. all internal lines of the diagrams are summed over including relativistic factors $1/(2\omega L^2)$ and under the constraint that the state E_i

[8] This constraint on the propagator applies when calculating the vacuum energy. The generalisation when the propagator is shifted by non-zero external energy is straightforward.

flowing between any two consecutive vertices is smaller than the energy cutoff, $E_i \leqslant E_T$. Even-though the diagram (3.16) is a permutation of the vertices of diagram (3.15), it is apparent that the expression in Eq. (3.15) differs from Eq. (3.16). The latter is finite as $E_T \to \infty$, while diagram (3.15) diverges logarithmically in the limit $E_T \to \infty$. Indeed,

$$(3.15) = \frac{g^3}{6} \sum \frac{L^2 \delta_{q+p,0}}{\omega_p + \omega_q} \sum \frac{L^2 \delta_{k_1+k_2+k_3+p,0}}{\omega_{k_1} + \omega_{k_2} + \omega_{k_3} + \omega_p} + O(m^2/E_T) \tag{3.17}$$

where the second factor $\sum \frac{L^2 \delta_{k_1+k_2+k_3,0}}{\omega_{k_1}+\omega_{k_2}+\omega_{k_3}} \sim \log(E_T)$. Further details and examples are given in appendix D.

For clarity, in each of the preceding diagrams we have drawn vertical lines cutting between consecutive vertices to signal the state propagating. We will not draw such lines in what follows. However, one should remember that the vertices of all the diagrams below are ordered.

3.2 Rules

The general rules to compute the first term in (3.1) can be summarised as follows. First, consider all possible Feynman diagrams for the transition $i \to i$, including both connected and disconnected diagrams. Now, draw each nth order Feynman diagram $n!$ times ordering the n vertices in every possible way, with the external lines kept fixed. Label each internal line with space momenta $\vec{p}$. Then the rules associated to each particular vertex-ordered diagram are

- For every vertex except the last [leftmost], include a factor L^2 times a momentum conservation Kronecker delta.
- For every intermediate state j, i.e. a set of lines between any to consecutive vertices, include a factor
$$[E_i - E_j + i\epsilon]^{-1} \tag{3.18}$$
where $E_j \equiv \sum \omega$ is the total energy of the state j.
- For every internal line include a factor $[(L^2(2\omega_{\vec{p}})]^{-1}$ while every external line counts a factor $[(L^2(2\omega_{\vec{p}})]^{-1/2}$.
- Multiply by $g^n/n!$ and by the symmetry factor associated to the diagram. If in doubt, resort to the general formula given in (3.6).
- Integrate the product of these factors over all the internal momenta.

Finally, sum all the expressions associated to the vertex ordered diagrams. The rules to compute the pieces in the subtraction terms are analogous, only differing in some extra powers of $(E_i - E_j + i\epsilon)^{-1}$ which are readily traced. In order to get (3.2) we need to remember not to include the state E_i in the sum over internal states, then the ϵ in (3.18) can be safely dropped. At infinite volume the internal lines are changed as $1/\left(L^2 2\omega_{\vec{p}}\right) \to 1/\left((2\pi)^2 2\omega_{\vec{p}}\right)$, the Kronecker deltas $L^2\delta_{\vec{k}} \to (2\pi)^2\delta^{(2)}(\vec{k})$ and the sums $\sum_{\vec{k}} \to \int d^2k$. The rules just described are similar to those to compute scattering matrix elements in Old Fashioned Perturbation Theory, see e.g. [21].

4 ϕ^2 test

In this section we apply Hamiltonian Truncation techniques to a mass perturbation ϕ^2 in $2+1$ dimensions. This perturbation is exactly solvable. It is nevertheless interesting to compare the exact solution with perturbation theory and HT since these latter two approaches are of much more general. In our detailed comparison with perturbation theory we will learn a lesson that will be crucial when generalising the HT method to the ϕ^4 perturbation.

4.1 Analytic solution

The free theory is given by the action

$$S_0 = \int d^3x \left(\frac{1}{2}(\partial\phi)^2 - \frac{1}{2}m^2\phi^2 + \frac{m^2}{2}Z \right) , \tag{4.1}$$

where $Z = \int \frac{d^3p}{(2\pi)^2} \frac{1}{p^2+m^2}$. The only potential divergence of the theory, which consists of a one loop diagram with a single mass insertion, is canceled by the $m^2 Z$ term. Thus, the vacuum energy of the theory in (4.1) is zero and the excited states are the free theory Fock states $|E_i\rangle$, with energies E_i. Next we perturb the theory by $m^2 \to m^2 + g_2$,

$$S_{g_2} = \int d^3x \left(\frac{1}{2}(\partial\phi)^2 - \frac{1}{2}M^2\phi^2 + \frac{M^2}{2}Z \right) , \tag{4.2}$$

with $M^2 = m^2 + g_2$. In the perturbed theory (4.2) the vacuum energy is non-zero and measurable. Indeed, the vacuum energy density is given by the effective potential

$$\mathcal{V}_{\text{eff}}(g_2) = \frac{2}{24\pi}\left[(m^2)^{3/2} - (m^2+g_2)^{3/2} + \frac{3}{2}g_2 m \right] , \tag{4.3}$$

where (4.3) only receives contributions from a single loop, i.e. the Coleman-Weinberg [22] potential $\mathcal{V}_{\text{eff}}(g_2) = \frac{1}{2}\int \frac{d^3p}{(2\pi)^2} \log(p^2+M^2) - M^2 Z$. The excited states are Fock space states with energy

$$L^2\, V_{\text{eff}}(g_2) + E_i \, , \tag{4.4}$$

where L^2 is the volume of the space. Eq. (4.4) is valid for large volumes, so that winding corrections can be ignored. [9]

4.2 Perturbative solution

Next we compute the first terms of the perturbative expansion of V_{eff} and of the mass gap $\Delta = \mathcal{E}_1 - \mathcal{E}_0$ using time ordered perturbation theory [for the calculations of this section we set $m = 1$]. We will do the calculation up to $O(g_2^4)$ where the effect that we want to discuss first arises for the vacuum energy. The conclusions that we draw in this section are insensitive to whether we work in finite or infinite volume, so we use the infinite volume phase space formula throughout.

[9] We do however include winding corrections in our subsequent comparison with HT calculations, since they have a small but not negligible effect for the box sizes we use.

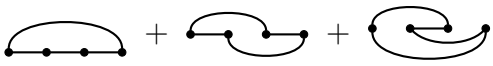
4.2.1 Vacuum

The vacuum is given by $\mathcal{E}_0 = \mathcal{E}_0^{(2)} + \mathcal{E}_0^{(3)} + \mathcal{E}_0^{(4)} + O(g_2^5)$. At $O(g_2^2)$ and $O(g_2^3)$ we have the contributions

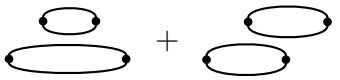

$$= \frac{g_2^2}{2}\int_2^\infty \frac{dE}{2\pi}\frac{\Phi_2(E)}{-E} = -\frac{g_2^2}{32\pi} \quad \text{and}$$

$$= \int_2^\infty \frac{dE}{2\pi}\frac{\Phi_2(E)}{E\cdot E^2} = \frac{g_2^3}{192\pi}\,. \tag{4.5}$$

At $O(g_2^4)$ we have three connected diagrams


$$= -\left(1+1+\frac{1}{2}\right)\int_2^\infty \frac{dE}{2\pi}\frac{1}{E^2\cdot E^3} = -\frac{g_2^4}{512\pi}\,, \tag{4.6}$$

and two disconnected diagrams


$$= -\frac{1}{4}\int_2^\infty \frac{dE_1}{2\pi}\frac{dE_2}{2\pi}\frac{\Phi_2(E_1)}{E_1+E_2}\frac{\Phi_2(E_2)}{E_2}\left(\frac{1}{E_1}+\frac{1}{E_2}\right) = -\frac{g_2^4}{256(4\pi)^2}\,, \tag{4.7}$$

all arising from the $VH_0^{-1}VH_0^{-1}VH_0^{-1}V$ piece. Meanwhile the second term of $\mathcal{E}_0^{(4)}$ in (3.2) gives a fully disconnected piece

$$-\mathcal{E}_0^{(2)}\,V_{0k}E_k^{-2}V_{k0} = \frac{g_2^2}{2}\int_2^\infty \frac{dE}{2\pi}\frac{\Phi_2(E)}{E}\frac{g_2^2}{2}\int_2^\infty \frac{dE}{2\pi}\frac{\Phi_2(E)}{E^2} = \frac{g_2^4}{256(4\pi)^2}\,. \tag{4.8}$$

As expected, the disconnected pieces cancel, (4.7) + (4.8) = 0; and adding up all the corrections we reproduce (4.3)

$$L^2\mathcal{V}_{\text{eff}} = -\frac{g_2^2}{32\pi} + \frac{g_2^3}{192\pi} - \frac{g_2^4}{512\pi} + O(g_2^5)\,. \tag{4.9}$$

The point of this exercise is to note that if we set up a sharp E_T cutoff on the energy of the states propagating in between the vertices, Eq. (4.7) is now given by

$$-\frac{1}{4}\int_2^{E_T-2}\frac{dE_2}{2\pi}\frac{\Phi_2(E_2)}{E_2^2}\int_2^{E_T-E_2}\frac{dE_1}{2\pi}\frac{\Phi_2(E_1)}{E_1} \tag{4.10}$$

while the integrals of (4.8) are cut off independently

$$\frac{1}{2}\int_2^{E_T}\frac{dE}{2\pi}\frac{\Phi_2(E)}{E}\frac{1}{2}\int_2^{E_T}\frac{dE}{2\pi}\frac{\Phi_2(E)}{E^2}\,. \tag{4.11}$$

Therefore, when the E_T cutoff is introduced, the disconnected diagrams do not cancel by terms of $O(1/E_T)$,

$$(4.10) + (4.11) = \frac{1}{512\pi^2}\frac{1}{E_T^2}\,. \tag{4.12}$$

This effect is harmless in practice for this theory because it decouples fast enough. However, these kind of effects will turn out to be very important for the ϕ^4 theory [or generic UV divergent theories] because for ϕ^4 theory the non-cancelation of disconnected bubbles is not suppressed by powers of E_T. This will be discussed in detail in section 5.

4.2.2 First excited state

To develop our intuition further, we now carry out the analogous calculation of the energy of the first excited state. We start by computing the connected diagrams, and then we compute the disconnected diagrams contributing to $\mathcal{E}_1$.

Connected diagrams. The leading correction to the first excited state $\mathcal{E}_1$ is given by $\mathcal{E}_1^{(1)} = V_{11} =$  $= \frac{g_2}{2}$. Next, at $O(g_2^2)$,

$$\mathcal{E}_1^{(2)}|_{\text{Conn.}} = \quad = -\frac{g_2^2}{8}\,, \tag{4.13}$$

meanwhile at $O(g_2^3)$ we find

$$\mathcal{E}_1^{(3)}|_{\text{Conn.}} = \quad + \quad + \quad = 3\frac{g_2^3}{8}\frac{1}{(1-3)^2} = 3\frac{g_2^3}{32} \tag{4.14}$$

Finally, there are several connected contributions at $O(g^4)$:

$$+ \quad + 2 \quad +2 \quad + 2 \quad + 2 \quad + \quad + \quad . \tag{4.15}$$

It is straightforward to compute these diagrams and we are led to

$$\mathcal{E}_1^{(4)}|_{\text{Conn.}} = -g_2^4\frac{11}{128} \tag{4.16}$$

Disconnected diagrams. There is a single diagram at $O(g_2^2)$ and it is equal to the $O(g_2^2)$ vacuum correction. At $O(g_2^3)$, we have various kinds of pieces arising from $V_{1k}E_{1k}^{-1}V_{kk'}E_{1k'}^{-1}V_{k'1}$. The first type is

$$\quad , \tag{4.17}$$

where the blob is fully connected and given in (4.5). Then we can also have

$$\quad = \frac{g_2}{2}\frac{g_2^2}{2}\int_2^\infty \frac{dE}{2\pi}\frac{\Phi_2(E)}{E^2} = \frac{g_2^4}{256\pi}\,, \tag{4.18}$$

which cancels with the disconnected 1-loop bubble of

$$-V_{11}\times V_{1k}(m-E_k)^{-2}V_{k1} = -\frac{g_2}{2}\times\left(\underbrace{\frac{g_2^2}{4}\frac{1}{(1-3)^2}}_{\text{tree}} + \underbrace{\frac{g_2^2}{2}\int_2^\infty\frac{dE}{2\pi}\frac{\Phi_2(E)}{E^2}}_{1-\text{loop}}\right), \tag{4.19}$$

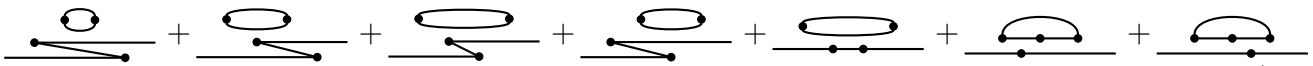
while the tree-level piece of the former equation combines with (4.14) to give $-g_2^3/16$.

At $O(g_2^4)$ the term $V\,[1/(m-H_0)V]^3$ gives rise to two types of disconnected contribution.



, (4.20)

where the bubble is fully connected $O(g^4)$ vacuum given in (4.6) – once the fully disconnected contribution from $-\mathcal{E}_1^{(2)}\,V_{1k}E_k^{-2}V_{k1}$ [proportional to π^{-2}] are added up. Meanwhile there are a number disconnected diagrams of the second type



, (4.21)

given by

$$-g_2^4\int_2^\infty\frac{dE}{2\pi}\Phi_2(E)\left(\frac{1}{8}\left[\frac{1}{4}\frac{1}{2+E}+\frac{1}{2E}\frac{1}{2+E}+\frac{1}{E^2}\frac{1}{2+E}+\frac{1}{2E}\frac{1}{2+E}+\frac{1}{2E^3}\right]+\frac{1}{E^4}\right)=-\frac{17g_2^4}{3072\pi},$$

where each summand in the $[\cdots]$ piece of the integrand corresponds to the five first diagrams in (4.21); while the last two in (4.21) correspond to the $1/E^4$ piece. Next we need to compute the fully disconnected pieces, there are three of them [the last three pieces of $\mathcal{E}_i^{(4)}$ in (3.2)]:

$$-\mathcal{E}_1^{(2)}\times[V_{1k}(1-E_k)^{-2}V_{k1}] = \left[\frac{g_2^2}{8}+\frac{g_2^2}{32\pi}\right]\times\left[\frac{g_2^2}{16}+\frac{g_2^2}{128\pi}\right], \tag{4.22}$$

$$-2V_{11}\times V_{1k}(1-E_k)^{-2}V_{kk'}(1-E_{k'})^{-1}V_{k'1} = g_2\times\left[3\frac{g_2^3}{64}+\frac{g_2^3}{768\pi}+\frac{g_2^3}{512\pi}\right] \tag{4.23}$$

$$V_{11}^2\times V_{1k}(1-E_k)^{-3}V_{k1} = -\frac{g_2^2}{4}\times\left[\frac{g_2^2}{32}+\frac{g_2^2}{384\pi}\right]. \tag{4.24}$$

Thus, we have that

$$(4.22)+(4.23)+(4.24)=\underbrace{\frac{3}{64}}_{\text{tree}}+\underbrace{\frac{17}{3072\pi}}_{1-\text{loop}}+\underbrace{\frac{1}{4096\pi^2}}_{2-\text{loop}}. \tag{4.25}$$

The two loop piece has already been accounted for in (4.20); the one-loop piece cancels against (4.21) [we have coloured terms that cancel each other]; while the tree-level piece combines with the connected tree-level diagrams in (4.16) to give $\mathcal{E}_1^{(4)}|_{\text{tree}}=-g_2^4\frac{5}{128}$. This again shows the importance of the subtraction terms in (3.1).

Adding all the contributions, we have

$$\mathcal{E}_1=m+\frac{g_2}{2m}-\frac{g_2^2}{8m^3}+\frac{g_2^3}{16m^5}-\frac{5g_2^4}{128m^7}+$$  $$+O(g^5), \tag{4.26}$$

where the blob involves fully connected vacuum diagrams.

The cancellation of disconnected bubbles is expected from Lorentz covariant perturbation theory. It is however interesting to note that in the non-covariant calculation, the cancellation of the disconnected bubbles appears non-trivial. Additionally, although disconnected bubble diagrams

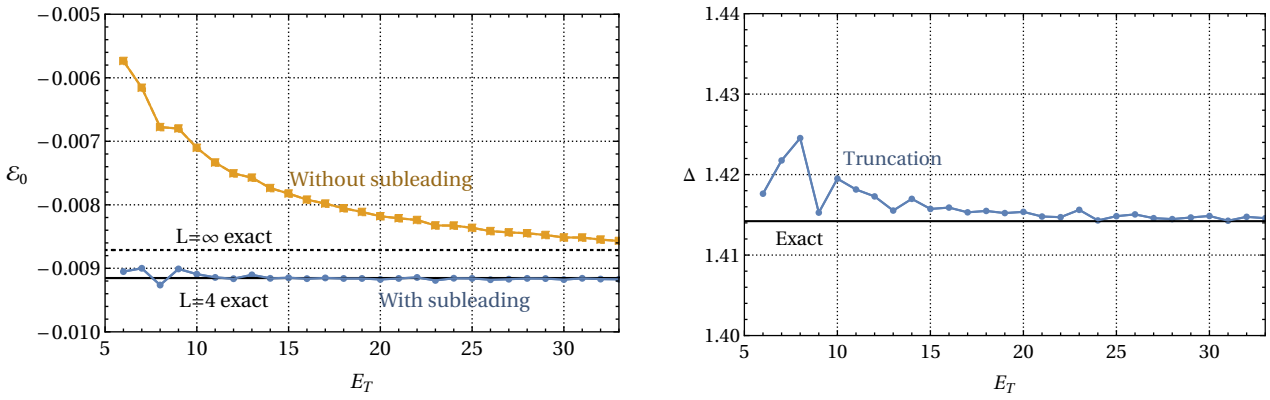


Figure 2: The vacuum energy density [left] and mass gap [right] of the theory defined by Eq. (4.1) deformed by Eq. (4.28) with $g_2 = 1$ as a function of the cutoff energy E_T. The analytic predictions both in the infinite volume limit and at finite volume are also indicated. The results for the vacuum energy are shown with and without including the sub-leading correction (4.29), which improves the convergence.

cancel out as $E_T \to \infty$, note that in HPT not all disconnected diagrams cancel. Indeed, the tree-level pieces of $O(g_2^3)$ and $O(g_2^4)$ involve disconnected tree-level diagrams [this is also expected since we are computing the mass gap instead of the mass-gap squared].

All in all, the mass gap is given by

$$\Delta \equiv \mathcal{E}_1 - \mathcal{E}_0 = m + \frac{g_2}{2m} - \frac{g_2^2}{8m^3} + \frac{g_2^3}{16m^5} - \frac{5g_2^4}{128m^7} + O(g_2^5) = \sqrt{m^2 + g_2} + O(g_2^5)\,, \tag{4.27}$$

which of course reproduces the result of a Lorentz covariant calculation. Our derivation of (4.27) with HPT is a very inefficient way to solve for the harmonic oscillator! However, Hamiltonian Truncation [which will require a detailed understanding of the cancelation of the disconnected bubbles] will turn out to be a very efficient way to solve for other theories that we do not know how to solve analytically.

4.3 Hamiltonian Truncation solution

As well as providing a useful theoretical warm up for what will follow, we can use the ϕ^2 perturbation as a first test of the Hamiltonian Truncation method. This is analogous to the analysis carried out in $1+1$ dimension in [9]. Starting from a Fock space basis of the theory in (4.1) we introduce a perturbation

$$\Delta H = g_2 V_2\,. \tag{4.28}$$

This simply corresponds to turning off g_4 in (2.2) with $m = 1$. Since the theory is UV finite, and the cancellation of bubble diagrams discussed around (4.12) is restored when taking the limit $E_T \to \infty$, [10] the counter-terms in (2.2) can be set to zero in this case. Extrapolating the values

[10] A proof of this statement at all orders in perturbation theory will be presented in section 5.1 and appendix B.2.

of the vacuum energy and the mass gap obtained from the diagonalisation to $E_T \to \infty$ the exact analytic results should be recovered.

In Figure 2 left we plot the vacuum energy density obtained from HT calculations as a function of E_T for a theory with $g_2 = 1$ and $L = 4$. For such a box the winding corrections to the exact vacuum energy are significant, and we show the analytic result both for an infinitely large box and including finite volume effects. The direct result from the truncation calculation is shown in orange [labeled "without sub-leading"]. Although this appears to be approaching the analytic result, at the accessible values of E_T it is not yet fully converged.

The convergence of the vacuum energy as a function of E_T can be improved by adding corrections to the truncated Hamiltonians. These account for the leading effects of states with $E > E_T$ that are missing from the computation, and vanish in the $E_T \to \infty$ limit. Such corrections have been studied extensively, starting with [23–25], continuing with the full systematic calculation in [9, 16], while further developments and the state of the art perspective can be found in [11, 13, 15, 17]. For our purposes we simply include the first correction, which scales as $1/E_T$ and arises due to the integral corresponding to the left diagram of (4.5) being cut off at E_T. The contribution "missing" from such a diagram due to the truncation is a shift in all of the energy levels of [11]

$$\Delta H_2 = \frac{-g_2^2}{4} \int_{E_T}^{\infty} \frac{dE}{2\pi} \frac{\Phi_2(E)}{E} = -\frac{g_2^2}{16\pi E_T} + O(1/E_T^2)\,, \tag{4.29}$$

which is easily incorporated as an additional diagonal term in the Hamiltonian matrix. The results with the sub-leading correction included are also plotted in Figure 3, and they converge much faster to the analytic result.

In Figure 2 right we show the mass gap in the same theory. The results obtained are unaffected by whether the diagonal correction (4.29) is included. Instead the leading correction to the mass gap is higher order in g_2 and E_T, and is not needed for our present purposes. We have also confirmed that the energies of the next few excited states quickly converge to their expected values.

In Figure 3 we plot the vacuum energy density and mass gap obtained in the limit $E_T \to \infty$ as the coupling g_2 is varied; the results are shown along with the analytic predictions at finite and infinite volumes. [11] The perturbative prediction at orders g_2^2 and g_2^4 is also plotted. We find good agreement between HPT and HT for perturbative values $g_2 \in (-1/2, 1)$, while HT agrees precisely with the exact calculation (4.4) for the entire range of couplings. Additionally we see that the truncation calculation is correctly capturing the winding corrections. It is encouraging that the truncation calculation is sensitive to high order diagrams of HPT, and that it gives precise results.

5 Hamiltonian Truncation for a UV divergent perturbation

Now we turn to our main concern: developing a formalism to apply HT to UV divergent relevant perturbations that require renormalisation. To do so, we analyse HPT with an E_T cutoff for the ϕ^4 perturbation in detail.

[11] In particular we fit the finite E_T data with a function of the form $\alpha_0 + \alpha_1/E_T$, where α_i are constants. Adding an extra $\alpha_i/E_T \log E_T$ or α_2/E_T^2 freedom in the fit does not affect the value of α_0 in any significant way.

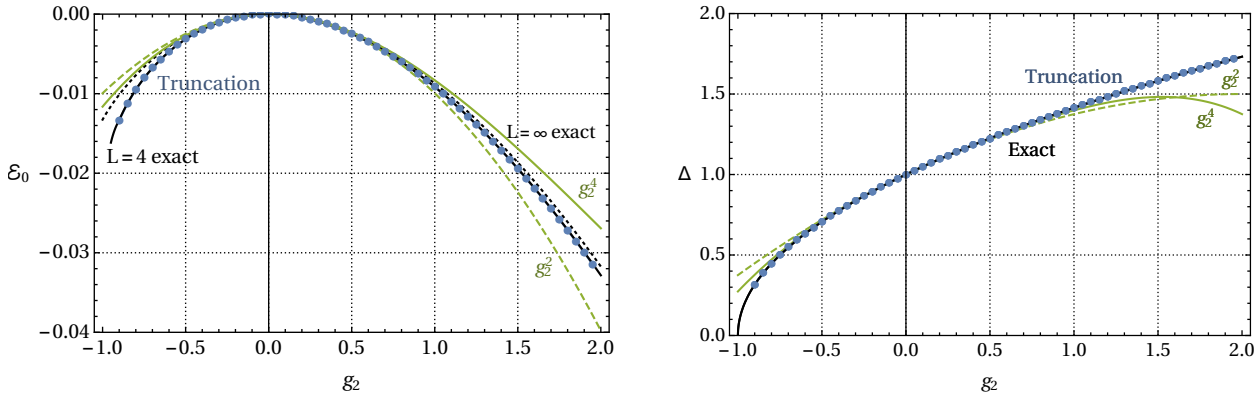


Figure 3: The vacuum energy density [left] and mass gap [right] as a function of g_2 obtained from Hamiltonian Truncation calculations after extrapolation to $E_T \to \infty$. We also show the exact analytic results [for the vacuum energy density with and without including winding corrections, solid and dashed respectively] and the prediction from perturbation theory [labeled PT] at order g_2^2 and g_2^4.

A straightforward inspection of the HPT Feynman diagrams reveals the presence of two primitive UV divergencies associated to the vacuum

$$= c_0(E_T) \sim \frac{-g^2 L^2}{96(4\pi)^3}\left(E_T - 8m\log\frac{E_T}{m}\right), \qquad = d_0(E_T) \sim \frac{g^3 L^2}{3072(4\pi)^2}\log\frac{E_T}{m}, \tag{5.1}$$

and one to the computation of the first excited energy level at $O(g^2)$,

$$\sim c_2(E_T) = -\frac{g^2}{6(4\pi)^2}\log\frac{E_T}{m}, \tag{5.2}$$

we call the latter the sunset diagram. [12] Thus we must add counter-terms to define a theory with a finite $E_T \to \infty$ limit. Tentatively, one may consider the following potential as a perturbation of the free massive theory

$$V \stackrel{?}{=} V_4 - c_0(E_T) - d_0(E_T) - c_2(E_T)V_2\ , \tag{5.3}$$

as one would do in a covariant calculation of correlation functions or scattering amplitudes. However, this theory does not have a finite $E_T \to \infty$ limit. Next we will prove this claim and we will identify the problems in doing a perturbative calculation with an E_T cutoff regulator.

We start by explaining in detail the calculation of the vacuum energy up to $O(g^4)$ in section 5.1. This analysis parallels the explanation in section 4.2.1 for the ϕ^2 perturbation, but with some key differences that will be stressed below. Subsequently, in section 5.2 we generalise this analysis to arbitrary order in perturbation theory. Following this, in section 5.3 we will solve the problems with perturbation theory, which will enable us to formulate Hamiltonian Truncation in section 5.4.

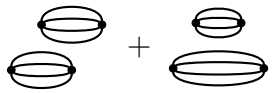
[12] Note that c_0 and d_0 are taken to be equal to the diagrams, while for c_2 we take the leading log. See appendix C for further details on the calculation of (5.1) and (5.2).

5.1 Problems with naive perturbation theory

The calculation of the vacuum at $O(g^2)$ and $O(g^3)$ is straightforward. There are only two connected diagrams, given in (5.1). In the theory of (5.3), the UV divergences associated to these diagrams are readily subtracted by lower order diagrams involving the counter-terms c_0 and d_0.

At $O(g^4)$, the calculation gets much more interesting. We discuss the disconnected diagrams first and then the connected diagrams. We have two disconnected pieces. The first piece, arising from the first term of $\mathcal{E}_0^{(4)}$ in (3.2), is given by

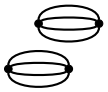
$$V_{0k_1}E_{0k_1}^{-1}V_{k_1k_2}E_{0k_2}^{-1}V_{k_2k_3}E_{0k_3}^{-1}V_{k_30}|_{\text{Disc.}} = \quad + \quad , \tag{5.4}$$



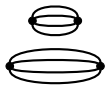
and formally cancels against the fully disconnected piece [i.e. second term of $\mathcal{E}_0^{(4)}$ in (3.2)]:

$$-\mathcal{E}_0^{(2)} \times V_{0k}E_k^{-2}V_{k0} = \frac{(gL)^2}{24}\int_4 \frac{dE}{2\pi}\frac{\Phi_4(E)}{E} \times \frac{(gL)^2}{24}\int_4 \frac{dE}{2\pi}\frac{\Phi_4(E)}{E^2}\,. \tag{5.5}$$

Indeed, the diagrams in (5.4) are given by



$$= -\frac{(gL)^4}{576}\int_4 \frac{dE_1}{2\pi}\frac{dE_2}{2\pi}\frac{\Phi_4(E_1)}{E_1+E_2}\frac{\Phi_4(E_2)}{E_1E_2}\,, \quad$$



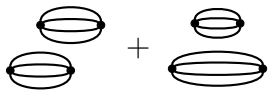
$$= -\frac{(gL)^4}{576}\int_4 \frac{dE_1}{2\pi}\frac{dE_2}{2\pi}\frac{\Phi_4(E_1)}{E_1+E_2}\frac{\Phi_4(E_2)}{E_2^2}\,, \tag{5.6}$$

and upon adding them the integrals in (5.4) neatly factorise as in (5.5). Note however that both (5.4) and (5.5) are UV divergent in $d = 2+1$ dimensions because

$$\Phi_4(x) = \frac{x}{128\pi^2} + O(x^0)\,. \tag{5.7}$$

Therefore, the former expressions require regularisation. If we proceed with a covariant regulator, e.g. cutting the momenta circulating in the loops, the cancellation of (5.4) + (5.5) = 0 still takes place [alternatively we can perform dimensional regularisation in position space (3.4), $D(x^\mu) = (2\pi)^{-d/2}(m/\sqrt{x_\mu^2})^{d-2}K_{(d-2)/2}(m\sqrt{x_\mu^2})$]. The problem arises if we insist on regularising the theory by restricting the Hilbert space to the states with a maximal H_0-energy E_T. Then, we must replace (5.5) and (5.6) with

$$-\mathcal{E}_0^{(2)} \times V_{0k}E_k^{-2}V_{k0} \;=\; \frac{(gL)^2}{24}\int_4^{E_T} \frac{dE}{2\pi}\frac{\Phi_4(E)}{E} \times \frac{(gL)^2}{24}\int_4^{E_T} \frac{dE}{2\pi}\frac{\Phi_4(E)}{E^2}\,, \tag{5.8}$$



$$= -\frac{(gL)^4}{576}\int_4^{E_T-4} \frac{dE_2}{2\pi}\frac{\Phi_4(E_2)}{E_2^2}\int_4^{E_T-E_2} \frac{dE_1}{2\pi}\frac{\Phi_4(E_1)}{E_1}\,. \tag{5.9}$$

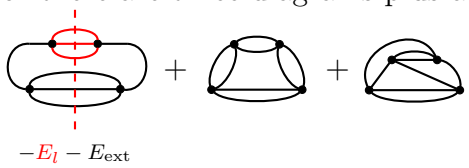
Now, when we add the previous two expressions we get

$$(5.8)+(5.9) = (gL)^4\frac{E_T - 8\log E_T}{144(8\pi)^6} + O(E_T^0)\,, \tag{5.10}$$

namely, disconnected diagrams do not cancel at finite E_T, and most importantly the effect does not decouple and diverges when the cutoff is removed!

In the connected sector there are three diagrams plus all their possible vertex orderings:

$$\mathcal{E}_0^{(4)}|_{\text{Conn.}} = \quad + \quad + \quad + \text{all vertex re-orderings} \tag{5.11}$$



Only the first diagram and its vertex re-orderings can be divergent. Indeed, the first diagram contains a UV divergent sub-sunset diagram [painted in red] for energies $E_l \sim E_T$. Note that the lower sunset sub-diagram propagating a state of energy E_{ext} is rendered convergent by the two vertex insertions [from the upper red sunset] in between its ends. The divergence in the upper sunset sub-diagram is taken care of by the counter-term c_2 at lower order in perturbation theory, and the divergences in the the vertex reordered diagrams are similarly cancelled. More generally, the connected vacuum diagrams are finite for the theory (5.3) at all orders in perturbation theory: *the only divergent sub-diagrams are sunset diagrams and these are subtracted by* c_2.

To sum up, the vacuum energy is equal to the sum of all connected vacuum Feynman diagrams. In HPT this is true because of delicate cancelations of the type (5.4) + (5.5) = 0. We have found that this cancelation is spoiled when we introduce the non-covariant regulator E_T.

Note that the problem of UV divergences due to disconnected bubbles discussed in this section is not present in ϕ^4 in $d = 1 + 1$ dimensions. Equations (5.8) and (5.9) are formally valid in any spacetime dimension, provided we use the appropriate phase space function,

$$\Phi_4^{d=1+1}(x) = \frac{H_1(4x^{-2}) - iH_2(4x^{-2}) + 3H_3(4x^{-2})}{8\pi^2} = \frac{3}{2\pi^2}\frac{1}{x^2}\left[\log^2(x) - \pi^2/12\right] + O(x^{-4})\,, \tag{5.12}$$

where the functions are H_i are given in terms of the Bessel function K.[13] We find

$$(5.8) + (5.9) \overset{d=1+1}{=} O(E_T^{-1})\,. \tag{5.13}$$

Therefore in previous ϕ_2^4 Hamiltonian Truncation studies [9] the problem in (5.10) did not arise.

5.2 The general case

The problem found in (5.10) is ubiquitous to all orders $O(g^n)$ in perturbation theory for $n \geqslant 4$. To identify all the diagrams that, as a result of the E_T cutoff, diverge in the $E_T \to \infty$ extrapolation we generalise the two separate UV divergent contributions in (5.9). In section 5.2.1, we discuss the generalisation of the second diagram in (5.4). Then, in section 5.2.2 we will deal with the generalisation of the first diagram in (5.4). [14]

The perturbative correction to the E_i state at $O(g^n)$ is given by

$$\mathcal{E}_i^{(n)} = \underbrace{\frac{V_{ik_1}V_{k_1k_2}\cdots V_{k_ni}}{E_{ik_1}E_{ik_2}\cdots E_{ik_{n-1}}}}_{\text{1st contribution}} \underbrace{- \mathcal{E}_0^{(2)}\frac{V_{ik_1}V_{k_1k_2}\cdots V_{k_{n-2}i}}{E_{ik_1}E_{ik_2}\cdots E_{ik_{n-3}}}\sum_{s=1}^{n-3}\frac{1}{E_{ik_s}} - \mathcal{E}_i^{(n-2)}V_{ik}E_{ik}^{-2}V_{ki} + \ldots}_{\text{2nd contribution}} \tag{5.14}$$

[13] One finds $H_1 = K(t_+(x))K(t_-(x))$, $H_2 = K(t_+(x))K(1 - t_-(x))$, $H_3 = -K(1 - t_+(x))K(1 - t_-(x))/3$ and $t_\pm(x) = 1/(4x)(2x + (1 - 2x)\sqrt{(x-1)/x} \pm \sqrt{(4x-1)/x})$.

[14] Most of the formulas of this section are valid in either finite or infinite volume (and d dimensions), provided the correct phase-space function Φ_4 is used.

where a sum over $k \neq i$ is implicit. In (5.14) ... denotes further corrections that are irrelevant for the current discussion – these are terms proportional to either V_{nn} or $\mathcal{E}_i^{(s)}$ with $3 \leqslant s \leqslant n-3$. The diagrams that we are presently interested in are obtained from the first contribution in (5.14) by considering each $O(g^{n-2})$ diagram [either connected or disconnected] with i external lines on each side of the diagram and dressing such diagram with two-point bubbles. We denote a generic diagram by , where the thick red lines represent any number of regular black lines.

The diagrams with a two-point bubble inserted in between every two consecutive vertices are represented by

 (5.15)

and the corresponding expression is given by

$$\int \prod_{a=1}^{n-3} \frac{dx_a}{x_{ia}}\, g_{E_i}(\vec{x}) \sum_{s=1}^{n-3} \frac{1}{x_{is}} \underbrace{\frac{(gL)^2}{24} \int_4^\infty \frac{dE}{(2\pi)} \frac{\Phi_4(E)}{E_i - (E + x_s)}}_{\text{two-point bubble + a free } |x_s\rangle \text{ state}}, \tag{5.16}$$

where x_s is the energy of the state being propagated in between any two consecutive vertices of the lower diagrams, and $x_{is} \equiv E_i - x_s$. There are $(n-2)-1$ such variables for a diagram with $n-2$ vertices. The function $g_{E_n}(\vec{x})$ depends on the specific lower diagram and includes a symmetry factor that is the same for each of the diagrams in (5.15). Eq. (5.16) is UV divergent because $\Phi_4(x) \sim x/(128\pi^2)$, thus we are assuming that (5.16) is properly regulated with e.g. a momentum cutoff.

Next we should add all the diagrams with the bubble's vertices in every other possible location. For instance, we must add diagrams such as

 (5.17)

After we add up all such diagrams, i.e. after dressing  with a two-point bubble in all possible ways, we find the following expression

$$\underbrace{\frac{(gL)^2}{24} \int_4^\infty \frac{dE}{(2\pi)} \frac{\Phi_4(E)}{E_i - E}}_{\text{two-point bubble}} \times \sum_{s=1}^{n-3} \int \prod_{a=1}^{n-3} \frac{dx_{ia}}{x_{ia}}\, g_{E_i}(\vec{x}) \Big(\sum_{s=1}^{n-1} \frac{1}{x_{is}} + \frac{1}{E_i - E} \Big), \tag{5.18}$$

i.e. the two-point vacuum bubble factors out. Therefore, the sum of all the dressings of each $O(g^{n-2})$ diagram by a two point bubble cancels with the second contribution in (5.14)! In appendix B we show how the factorisation and cancelation of the disconnected bubble takes place in detail. Although this is expected on general grounds [15], it is interesting to see how it happens in HPT and how it fails to happen when we regulate our theory with the E_T cutoff.

[15] See e.g. Chapter 16 of Weinberg vol. II [26].

5.2.1 *Two-point bubbles I*

When we regulate (5.16) with an E_T cutoff we get

$$\int \prod_{a=1}^{n-3} \frac{dx_a}{x_{ia}}\, g_{E_i}(\vec{x}) \sum_{s=1}^{n-3} \frac{1}{x_{is}} \frac{(gL)^2}{24} \int_4^{E_T - X_s} \frac{dE}{(2\pi)} \frac{\Phi_4(E)}{E_i - (E + x_s)}\,, \tag{5.19}$$

where $X_s = x_s$. It is useful to keep X_s and x_s as independent variables because, while the X_s dependence is due to the E_T regularisation, the x_s dependence is physical. Then, X_s will allow us to track by how much (5.19), once added to the rest of the two-point bubble dressings (5.17), fails to cancel against the fully disconnected *second contribution* of (5.14).

The important question however is by how much the former expression spoils the cancelation of disconnected two point bubbles as $E_T \to \infty$. To answer this, we can focus on a particular diagram contribution to (5.19) where the bubble is inserted on top of the sth propagating state. Then expanding at large E_T, we get

$$\int \prod_{a=1}^{n-3} \frac{dx_a}{x_{ia}} \frac{g_{E_i}(\vec{x})}{x_{is}} \frac{(gL)^2}{24} \Big[\underbrace{\frac{X_s - E_T}{256\pi^3}}_{\text{first term}} + \alpha_0 + \underbrace{\frac{X_s(-4-\alpha_{-1}) + \alpha_{-1}^2}{256\pi^3\, E_T}}_{\text{second term}} + O(E_T^{-2}) \Big]\,, \tag{5.20}$$

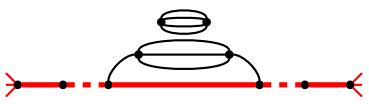
where α_0 and α_{-1} are functions of x_{is} and are readily computed using the phase-space formula (3.10). [16]

Therefore we are led to analyse which diagrams , when dressed with two-point bubbles in between two consecutive vertices, are sensitive to X_s. Nicely, in light of (5.20), the list of such type of diagrams is rather short. Indeed, only those diagrams $\mathcal{D}$ that are UV divergent – when the energy of one of the propagating states $X_s \sim E_T$ – will probe the X_s dependence in (5.20) when dressed with a two-point bubble in between two consecutive vertices. The non-cancellation of such diagrams against the subtraction terms leads to UV divergences not accounted by the counter-terms in (5.1)-(5.2). This is clear because, having identified the parts of (5.19) that are sensitive to the E_T regulator, we can restore $X_s = x_s$, and the dependence cancels off as

$$(5.20) = \int \prod_{a=1}^{n-3} \frac{dx_a}{x_{ia}}\, g_{E_i}(\vec{x}) \left[\frac{\cancel{x_{is}^{-1} X_s}}{256\pi^3} \frac{(gL)^2}{24} + O(X_s^0, X_s/E_T) \right], \tag{5.21}$$

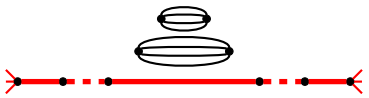
and we are left with the diagram $\mathcal{D}$ without the two-point bubble dressing, i.e. $\int \prod_{a=1}^{n-3} dx_a\, x_{ia}^{-1}\, g_{E_i}(\vec{x})$.

For instance the following diagram probes the *first term* in (5.20),

 . (5.22)

[16] We get $\alpha_{-1} = 4 - E_i + x_s$ and $\alpha_0 = \frac{4-\alpha_{-1}-4\log 4+(4-\alpha_{-1}^2/4)\log E_T+[\alpha_{-1}^2/4]\log \alpha_{-1}}{(4\pi)^3(4-\alpha_{-1})}$.

Indeed, the sunset diagram involves $g_{E_i}(\vec{x}) \sim O(x_s^0)$ because $\Phi_3(x) \sim O(x^0)$. Following the same logic, all those diagrams $\mathcal{D}$ that produce $g_{E_i}(\vec{x}) \sim O(x_s^1)$ will be sensitive to the *second term*, as well as the *first term*, in (5.20). For instance,



(5.23)

produces $g_{E_i}(\vec{x}) \sim O(x_s^1)$ because of the phase space growth $\Phi_4(x) \sim x/(128\pi^2)$ at large x. The instance in (5.23) is a straightforward generalisation of the right hand diagram in (5.6). [17]

So far we have analysed all the extra UV divergent terms that are produced when we regulate diagrams that contain a two-point vacuum bubble in between two given vertices with the E_T cutoff. To conclude the analysis we need to analyse the cases where the disconnected vacuum bubble spans one or more vertices as in for instance the diagrams in (5.17). This is the topic of next section.

5.2.2 Two-point bubbles II

We continue by analysing all diagrams consisting of a bubble crossing a single vertex,



(5.24)

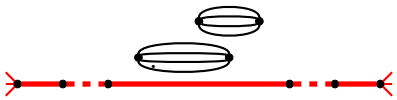
This expression is given by

$$\int \prod_{a=1}^{n-3} \frac{dx_a}{x_{ia}}\, g_{E_i}(\vec{x}) \sum_{s=1}^{n-3} \frac{(gL)^2}{24} \int_4^{E_T - X_s} \frac{dE}{(2\pi)} \frac{\Phi_4(E)}{[E_i - (E + x_{s-1})][E_i - (E + x_s)]}\,, \tag{5.25}$$

where $x_0 = 0$ and $X_s = \max\{x_{s-1}, x_s\}$, and we have regulated the divergent dE integral with the E_T cutoff. Again, we analyse the spurious divergences that are introduced with this regularisation by expanding at large E_T.

$$(5.25) = \int \prod_{a=1}^{n-3} \frac{dx_a}{x_{ia}}\, g_{E_i}(\vec{x}) \sum_{s=1}^{n-3} \frac{g^2}{24} \left[\beta_0 + \frac{(\beta_{-1} - X_s)}{256\pi^3\, E_T} + O(E_T^{-2})\right], \tag{5.26}$$

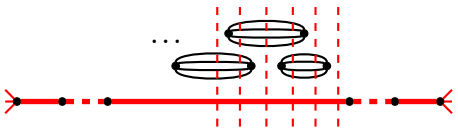
where β_i are functions of E_T and x_s but independent of X_s. In order to probe the coefficient of X_s in (5.26) and generate a UV divergence, the lower diagram must diverge as $\sim E_T^\alpha$ with $\alpha \geqslant 1$, i.e. we need $g_{E_i}(\vec{x}) \gtrsim x_s$. This for instance can be achieved if the vertex below the bubble in (5.24) is part of another two point bubble,



(5.27)

More generally iterated bubble diagrams also generates a linear divergence

[17] Note that since $c_0 \sim E_T - 8m \log E_T$, the second term in (5.20) spoils the cancelation of disconnected bubbles by finite $O(E_T^0)$ pieces.



(5.28)

where vertical lines are drawn to guide the eye to the propagating states. Iterated bubble diagrams of the form (5.28) are the only type of diagrams that diverge as $\sim E_T^\alpha$ with $\alpha \geqslant 1$, in particular they have $\alpha = 1$. This completes the generalisation of the left hand diagram in (5.6).

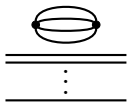
Note that two-point bubbles spanning more than one vertex do not introduce new UV divergences. In such case, the bubble is rendered log divergent at most. Then, the difference between cutting the integrals at E_T or $E_T - X_s$ is suppressed by E_T.

Thus, we have concluded the identification of all those diagrams for which the E_T regulator leads to extra UV divergences, which would not be present in a covariant scheme. All in all, these are diagrams of the form (5.15) and (5.28). [18]

5.2.3 Further comments

From the previous discussion it is clear that there are further diagrams that have a sensitivity to the non-covariant cutoff that scales as E_T^0, i.e. remains finite, in the large E_T limit. Such finite pieces are potentially problematic since they will make it challenging to match a Hamiltonian Truncation calculation with a covariant calculation. Consequently, we now examine some examples of diagrams that do and do not lead to finite corrections.

For instance, a source of finite $O(E_T^0)$ terms comes from the the correction to the energy of an n-particle state [with unperturbed energy E_n] by the disconnected g^2 bubble of (5.1), i.e.

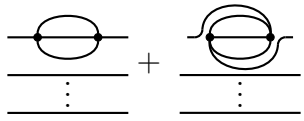
$$\mathcal{E}_n^{(2)} \supset$$  $$- c_0(E_T) L^2 \,, \tag{5.29}$$

where the diagram shifts the energy level by $\Delta E_n = \frac{(gL)^2}{24} \int_4^{E_T - E_n} dE \Phi_4(E)/(2\pi E)$. The UV divergence is canceled by $V_{nn} = c_0\,(E_T)\,L^2$, leaving a finite piece

$$\Delta E_n - c_0 L^2 = \left(-\frac{\log 2}{384\pi^3} + \frac{1}{6144\pi^3} E_n \right) g^2 L^2 \,. \tag{5.30}$$

This is due to the linear divergence present in the two-point bubble. Such a finite piece is not expected if a covariant scheme is used, namely a regulator that cuts the loop in (5.29) independently of the state flowing below.

Note that the sunset diagram does not lead to an analogous effect because it is only log divergent. For example, consider the diagrams

$$\mathcal{E}_n^{(2)} \supset$$  $$- c_2(E_T) \,, \tag{5.31}$$

[18] Strictly speaking we have only discussed those diagrams arising from the *first contribution* of (5.14). Note however that those diagrams arising form the *subtraction terms* in (3.1) have either equal or softer UV properties due to the extra factors $[E_i - E_j + i\epsilon]^{-1}$.

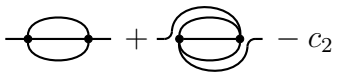
which are given by

$$\frac{1}{6}\int_3^{E_T-X}\frac{dE}{2\pi}\frac{\Phi_3(E)}{E_n-(E+x)}+\frac{1}{6}\int_3^{E_T-2-X}\frac{dE}{2\pi}\frac{\Phi_3(E)}{E_n-(E+2+x)}\,, \tag{5.32}$$

where x is the energy of the state below the loop, and $X=x$, but it is useful to treat them as independent variables. We are led to

$$(5.32)-c_2(E_T)=-\frac{\log(E_T/[3-E_n+x])}{96\pi^2}-\frac{\log([3-E_n+x]/3)}{32\pi^2(E_n-x)}+O(XE_T^{-1},E_T^{-1})\,, \tag{5.33}$$

namely there is no dependence on $X\times O(E_T^0)$. This is in accord with covariant regularisation. For instance, we may regulate the integrals in dimensional regularisation, or simply by $dE\to dE\,(\mu/E)^\epsilon$ with $\epsilon>0$. Then, the c_2 counter-term is given by $c_2(\epsilon)=-1/(96\pi^2\epsilon)$, such that the calculation of

 $-\,c_2$ (5.34)

is matched in either the E_T cutoff or $dE\,(\mu/E)^\epsilon$ scheme with $\mu=m$ [and using respectively $c_2(E_T)$ or $c_2(\epsilon)$]. But, the point is that once we fix the c_2 countertem such that (5.34) matches in the E_T and ϵ schemes, other diagrams like the ones in (5.31) automatically match in the two schemes. Indeed, upon performing the following integrals

$$\frac{1}{6}\int_3^{\infty}\frac{dE}{2\pi}\frac{\mu^\epsilon}{E^\epsilon}\frac{\Phi_3(E)}{E_n-(E+x)]}+\frac{1}{6}\int_3^{\infty}\frac{dE}{2\pi}\frac{\mu^\epsilon}{E^\epsilon}\frac{\Phi_3(E)}{E_n-(E+2+x)}-c_2(\epsilon)\,, \tag{5.35}$$

we find $\lim_{ET\to\infty}(5.33)=\lim_{\epsilon\to0}(5.35)|_{\mu=m}$.

We note however, that the sunset diagram can lead to finite $O(E_T^0)$ pieces when a two-point vacuum bubble spans one of or both its vertices. For example, consider embedding the sunset diagram in a diagram [either connected or disconnected] such that its two vertices are consecutive in time. These type of diagrams are given by

$$\int\prod_{i=1}^{n-3}\frac{dx_i}{x_i}\,g_{E_n}(\vec{x})\,\frac{1}{x_s}\frac{g^2}{6}\int_3^{E_T-X_s}\frac{dE}{2\pi}\frac{\Phi_3(E)}{E_e-(E+x_s)}\,, \tag{5.36}$$

where again $X_s=x_s$ but it is again useful to keep them independent to distinguish the scheme dependent pieces. The sensitivity to X_s for large E_T is

$$\Delta_s=\int\prod_{i=1}^{n-3}\frac{dx_i}{x_i}\,g_{E_n}(\vec{x})\,\frac{1}{x_s}\frac{g^2}{192\pi^2}\left(\frac{X_s}{E_T}+O\left(E_T^{-2}\right)\right)\,. \tag{5.37}$$

If a disconnected two-point bubble with energy x_s spans the sunset diagram $g_{E_n}(x_s)\sim x_s$, which leads to a finite piece in the large E_T limit. Meanwhile if, with the sunset bubble removed, the diagram is convergent or log divergent Δ_s vanishes in the large E_T limit.

If the vertices that comprise the sunset diagram are not consecutive in time, the degree of divergence is lowered. No such diagrams lead to new UV divergences, although those in which a

two-point disconnected bubble spans one of the sunset vertices give a finite regulator dependent piece.

By virtue of the fairly weak divergences in our chosen theory there are only a handful of types of diagrams where an $O(E_T^0)$ piece, not present in covariant regularisation, is generated after removing the cutoff $E_T \to \infty$. Further details are provided in appendix F.

5.3 Patching up perturbation theory with E_T regularisation

At this point we have nailed down the problems with perturbation theory in the E_T regularisation scheme precisely. All of the issues have a common origin: the problem of missing states! Namely, if a loop of energy E_l appears as a sub-diagram of HPT, then it belongs to a state propagating between two vertices that contains other particles of total energy E_{ext}. The E_T cutoff restricts the energy of the propagating state to $E_l + E_{\text{ext}} \leqslant E_T$. Therefore E_l explores energies strictly below E_T, which does not coincide with the energy being probed by the primitive UV divergencies that we identified in (5.1) and (5.2). Instead, if all loops were democratically cut at energy E_T the counter-terms (5.1) and (5.2) would be sufficient to a obtain a finite theory in the $E_T \to \infty$ limit.

We will now fix all these problems. We will do so by ensuring that all loop diagrams that have a UV divergent sensitivity to the regulator are effectively cut equally at E_T. Such diagrams involve the two point bubble inserted with its vertices sequential in time (5.15) and towers of the two point bubbles (5.28). As we argued above, if the loops of the disconnected two point bubbles are cut at E_T, the cancelation of such disconnected diagrams against the subtraction terms in (3.1) is automatic.

5.3.1 Patch I

First, we show how the effects of the states that are missing from the two point bubble diagram with vertices that are consecutive in time can be accounted for. We introduce a state dependent counterterm that is given by

$$\delta V^I_{nn,i} = \quad = \frac{g^2}{24}\int_{E_T-x_n}^{E_T}\frac{dE}{2\pi}\frac{\Phi_4(E)}{E_i-(x_n+E)} \,. \tag{5.38}$$

Note that, due to the appearance of E_i, the counter-term depends on which energy level is being calculated.

Considering the *1st contribution* at each order in perturbation theory in (5.14): For any diagram involving a two point bubble we can immediately write a diagram at the next order down in perturbation theory where the two vertices that make up the bubble are replaced by a single insertion of V_{nn}:



(5.39)

The former two diagrams replace (5.19) by

$$(5.39) = \int\prod_{a=1}^{n-3}\frac{dx_a}{x_{ia}}\,g_{E_i}(\vec{x})\sum_{s=1}^{n-3}\left(\frac{1}{x_{is}}\frac{(gL)^2}{24}\int_4^{E_T-X_s}\frac{dE}{(2\pi)}\frac{\Phi_4(E)}{E_i-(E+x_s)}+\frac{1}{x_{is}}\delta V^I_{ss}\right) . \tag{5.40}$$

The role of δV^I_{nn} is to account for the states that are missing due to the non-covariant regulator, so that the X_s dependence in (5.40) is removed. Note that $V_{00} = 0$ since no states are missing in this case.

The counterterm (5.38) also patches up the same problem in the *2nd contribution* of (5.14), i.e. the subtraction terms in (3.1). At order n in perturbation theory this includes expressions of the form

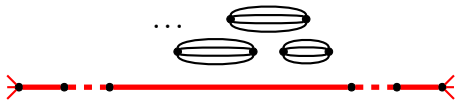
$$\mathcal{E}_0^{(j)} \frac{V_{ik_1} V_{k_1 k_2} \cdots V_{k_{n-j-1} i}}{E_{ik_1} E_{ik_2} \cdots E_{ik_{n-j-1}}} \sum_{s=1}^{n-j-1} \frac{1}{E_{ik_s}} \,. \tag{5.41}$$

States missing from two-point bubbles inside $\mathcal{E}_0^{(j)}$ are corrected for by a similar term at order $n-1$ that has a prefactor $\mathcal{E}_0^{(j-1)}$ containing δV^I_{nn}. For example, for $j = 2$ this amounts to simply replacing $\mathcal{E}_0^{(2)}$ with δV^I_{nn}. Two-point bubbles appearing in the second factor in (5.41), i.e. the part involving $V_{ik_1} \cdots V_{k_{n-j-1} i}$, are only dangerous if they do not have the extra propagator on them. These are patched up by insertions of δV^I_{nn} in the second factor of terms at the next order down.[19] At high order there are subtraction terms similar to (5.41) involving multiple factors of $\mathcal{E}_0^k$, but these are still patched up in the same way.

This exhausts all of the places that a two point bubble [with vertices consecutive in time] can be missing states in the perturbation theory, and also all of the places that the counterterm (5.38) can be inserted. Hence, (5.38) is sufficient to completely fix the problem we laid down in 5.2.1.

5.3.2 Patch II

The second issue to address is how to obtain a theory without a UV divergent sensitivity to the missing states of diagrams involving towers of overlapping two point bubbles (5.28),



(5.42)

As we argued above, these diagrams are problematic if we regulate with an E_T cutoff. The bubble integrals of former diagram are schematically given by

$$\int_4^{E_T - x_s} dE_1 \int_4^{E_T - x_s - E_1} dE_2 \int_4^{E_T - x_s - E_1 - E_2} dE_3 \frac{\Phi_4(E_1)}{E_1} \frac{1}{E_1 + E_2} \frac{\Phi_4(E_2)}{E_2} \frac{1}{E_2 + E_3} \frac{\Phi_4(E_3)}{E_3} \cdots \,, \tag{5.43}$$

where x_s is the energy of the state below the iterated bubbles, and we have dropped the dependence on the eigenstate E_i and x_s on the energy denominators.

A moment of thought reveals that this problem is hard to solve with a simple counter-term that can be written in closed form. [20] We instead offer a pragmatic solution, while we look forward to more elegant solutions in the future. We proceed in a similar fashion as we did in the previous

[19] Two point bubbles with an extra propagator on are not patched, but these are logarithmically divergent so only lead to finite corrections due to the E_T regulator.

[20] For instance, one may be tempted to correct the quartic coupling in a way that modifies all of its a^4, $\left(a^\dagger\right)^4$ etc. components, but we have found this not to work.

section, i.e. we introduce a further state-dependent vacuum counter-term, to account for the missing states in (5.42)

$$\delta V_{nn}^{II} = \frac{(gL)^4}{24^2}\left(\int_4^{E_T} dE_1 \int_4^{E_T} dE_2 - \int_4^{E_T-x_s} dE_1 \int_4^{E_T-E_1-x_s} dE_2\right) I(E_1, E_2) + \cdots \tag{5.44}$$

where we have only explicitly written the expression corresponding to two iterated bubbles, and the integrand is given by

$$I(E_1, E_2) = \frac{\Phi_4(E_1)\Phi_4(E_2)}{[E_i - (E_1 + x_s)][E_i - (E_1 + E_2 + x_s)][E_i - (E_2 + x_s)]} \,. \tag{5.45}$$

It is straightforward to write down the integral expression for a tower containing n iterated bubbles, denoted by the dots in (5.44).

The counter-term in (5.44) can be computed in a numerical code up to arbitrarily large numbers of bubbles. In our implementation below we patch up diagrams involving up to five overlapping bubbles, i.e. order g^{10}. The results that we obtain are not sensitive to including corrections corresponding to patching up larger numbers of bubbles. This indicates that the remaining cutoff dependence is not dominating our results.

5.3.3 Comment on off-diagonal counter-terms [17]

Ref. [17] stressed a potential problem with off-diagonal counter-terms. The main point is the following. Let us divide our potential as $V \to V + C^{(2)} + C^{(3)}$, where $C^{(n)}$ is a counter-term operator of $O(g^n)$ and $V = O(g)$. On one hand, the order $O(g^2)$ correction to the energy levels is

$$V_{ik}E_{ik}^{-1}V_{kj} + C_{ij}^{(2)} \,, \quad \text{with} \quad i = j \,, \tag{5.46}$$

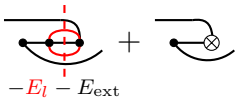
where recall that a sum over $k \neq i$ is implicit. The off-diagonal terms of $C^{(2)}$ are not fixed by demanding that (5.46) is finite when the regulator is removed. On the other hand the third order correction to the energy levels reads

$$V_{ik}E_{ik}^{-1}V_{kk'}E_{ik'}V_{k'i} + C_{ik}^{(2)}E_{ik}^{-1}V_{kj} + V_{ik}E_{ik}^{-1}C_{kj}^{(2)} + C_{ii}^{(3)} - \text{subtraction terms}\,. \tag{5.47}$$

Thus the $O(g^3)$ correction to the energy levels is sensitive to the off-diagonal terms of $C^{(2)}$. Now, a natural question arises about whether we should take care about the off-diagonal terms of $C_{ij}^{(2)}$. Or more generally, what is the structure of UV divergences in (5.47). [21]

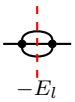
Let us rephrase the problem from the perspective of our detailed diagrammatic understanding. We consider the $g_2\phi^2 + g_4\phi^4$ theory in d dimensions as an instance, although similar comments apply more generally. As we have argued above if a hard cutoff in the Hilbert space is used [like E_T], divergent loops embedded in larger diagrams are cut at energies strictly below the cutoff [for instance see the first diagram in (5.11)]. Now it is not hard to imagine a sub-divergence arising from an off-diagonal term of $C^{(2)}$. For instance, consider the following $O(g_2 g_4^2)$ correction to the one particle state's mass

[21] The *subtraction terms* in (5.47) are independent of $C^{(n)}$ and thus irrelevant for our main point.



(5.48)

where $\otimes$ denotes the counter-term. Indeed, $C^{(2)}$ involves a diagonal correction to cancel the divergence from diagrams like



(5.49)

correcting the one particle state at $O(g_4^2)$.

We see the problem of off-diagonal counter-terms as an instance of the problem of missing states. Namely if the energy being propagated in between two consecutive vertices is cut at E_T, then the energy of the state being propagated in a loop depends on where the lines external to the loop end [these external lines are either or not attached to the loop].

For instance, returning to the example above, the loop in (5.48) is cut at $E_l \leqslant E_T - E_{\rm ext}$ with $E_{\rm ext} = 2m$, while the loop in (5.49) is cut at $E_l \leqslant E_T$. At this order this difference amounts to a finite scheme piece. However, after embedding these diagrams in higher order ones, $E_{\rm ext}$ may belong to an energy of another loop. Then, if $d \geqslant 7/2$ the sunset diagram is power like divergent; and the remaining $E_{\rm ext}$ that is left un-cancelled probes E_T energies and introduces new UV divergences. In this case, one must define a counter-term that captures this effect, i.e. that adds up the missing chunk of states $E_{\rm ext}$ to the loop in (5.48). For the theory we study in this paper [ϕ^4 in $d = 3$], the sunset is logarithmically divergent, thus the differences between $E_l \leqslant E_T - E_{\rm ext}$ and $E_l \leqslant E_T$ are $O(1/E_T)$; while the vacuum diagrams do generally suffer from the problem of missing states [although not necessarily due to off-diagonal contributions of $C^{(2)}$] as was carefully analysed in the sections above. Finally, we stress that if a regulator cuts all the loops equally [like covariant regulators do] the problem of missing states does not arise.

5.4 Hamiltonian Truncation formulation

Having understood perturbation theory with E_T cutoff regularisation and its large E_T extrapolation, we are now finally in the position to uplift the perturbative formulation into Hamiltonian Truncation. Thus, we will perturb the free massive theory by

$$V = V_4 - c_2(E_T)V_2 - \Omega(E_T) \quad \text{with} \quad \Omega(E_T) = c_0 + d_0 - \delta V^I - \delta V^{II} \,. \tag{5.50}$$

The counter-terms c_0, d_0 and c_2 were given in (5.1)-(5.2), for reference:

$$c_0(E_T) \sim \frac{-g^2L^2}{96(4\pi)^3}\left(E_T - 8m\log\frac{E_T}{m}\right), \quad d_0(E_T) \sim \frac{g^3L^2}{3072(4\pi)^2}\log\frac{E_T}{m}, \quad c_2(E_T) = \frac{-g^2}{6(4\pi)^2}\log\frac{E_T}{m}\,.$$

The c_0 and d_0 counter-term includes $1/E_T$ pieces to improve the convergence, the exact form is given in the appendix C. We will denote the vacuum and mass counter-terms vertices by $\otimes$. The corrections δV^I and δV^{II} are given in (5.38) and (5.44), respectively. Their role is to add back missing states that are cut away by the E_T regulator. We denote both such corrections by $\oplus$.

One difference compared to the ϕ_3^2 test in section 4 is that the counter-terms that add back missing states depend on the unperturbed external energy. For example, (5.38) depends on E_i.

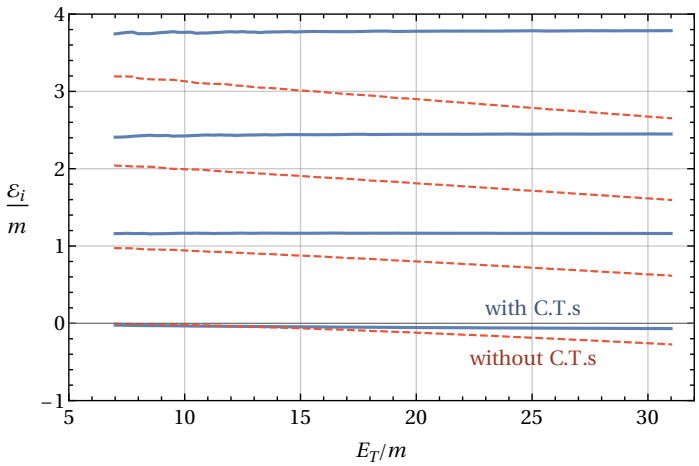


Figure 4: The vacuum and low lying energy levels of ϕ_3^4 obtained from a HT calculation as a function of the cutoff E_T, for a theory with $g = 18m$ in a box of size $L = 4/m$. We show the results with the compete set of counter-terms needed to render the theory finite ["with C.T.s"], and those obtained when no counter-terms are included ["without C.T.s"].

Therefore, a separate diagonalisation must be carried out to determine each energy level in the perturbed theory.

We have only shown that the interaction in (5.50) leads to a finite spectrum as $E_T \to \infty$ in perturbation theory. However, having reached this point we will press on and implement (5.50) in a numerical routine. We will find that the method gives sensible results for both perturbative and also moderately strong couplings.

6 Results from truncations

Next we implement the theory described in section 5.4 in a numerical code. First we study the dependence of the results from HT calculations on E_T, then we compare the results for the mass gap extrapolated to $E_T \to \infty$ with the perturbative prediction.

E_T dependence

In Figure 4 we show the results obtained for the vacuum energy and the energies of the first three excited states as a function of E_T, for the theory with $g = 18m$ and $L = 4/m$. It is clear that without counter-terms the energy levels of the theory do not converge, and once the counter-terms are included they are well converged. There are small fluctuations in the data, and these are only significant at $E_T \lesssim 15m$.

Notably the vacuum energy only deviates slightly from zero in Figure 4. This happens because the theory is fairly perturbative. We estimate the coupling g^* above which the theory is strongly coupled by demanding that $\mathcal{E}_0^{(3)} = \mathcal{E}_0^{(2)}$ at this value, leading to $g^* = 8.3$ [see below for further

details]. Since g is comparable to g^* and we subtract the exact vacuum diagrams up to order g^3, including their E_T dependence, we have $\mathcal{E}_0 \simeq 0$.

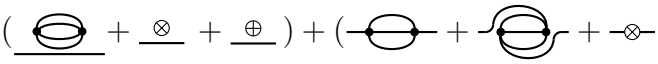
The higher energy levels are also extremely flat as a function of E_T, although they differ significantly from their classical values [i.e. from their values at order g^0]. Such behaviour can be understood from the evaluation of the g^2 correction to the mass gap at finite E_T [this is plotted in Figure 9 left of appendix G]. There is a finite correction at order g^2 as $E_T \to \infty$, and at $E_T \simeq 10$ this is within 10% of its asymptotic value. The correction to the mass gap at g^3 converges much more slowly, but for $g = 18m$ it is a factor of 6 smaller than the g^2 piece. In section 7 we will show data that indicates that the mass gap also converges at strong coupling, albeit more slowly.

Comparison with perturbation theory

As a cross check of the truncation calculations we compare the results obtained at weak coupling to the perturbative prediction. To do so we compute the mass gap up to order g^3 in perturbation theory. The diagrams that contribute to the vacuum energy at order g^2 are

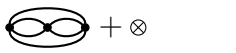
$\mathcal{E}_0^{(2)} =$  , (6.1)

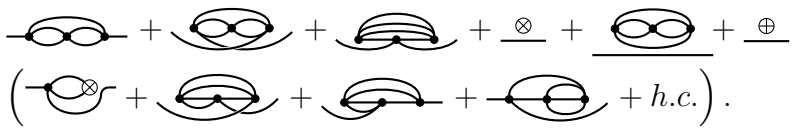
and the first excited level gets corrections from

$\mathcal{E}_1^{(2)} =$  , (6.2)

where $\oplus$ represents the counterterm that adds back in the missing states to the 2-point bubble divergence. Note that due to adding these states back in, the diagrams in the first bracket of (6.2) are equal to the shift in the vacuum energy of (6.1). Consequently the g^2 correction to the mass gap comes solely from the diagrams in the second bracket of (6.2).

Meanwhile at g^3 in perturbation theory the mass gap gets corrections from the diagrams

$\mathcal{E}_0^{(3)} =$  (6.3)

$\mathcal{E}_1^{(3)} =$  (6.4)

We evaluate the preceding diagrams with Monte Carlo integration for a box length $L = 4/m$. The mass gap is given by

$$\mathcal{E}_1 - \mathcal{E}_0 = m + 0.62\ [g/(4!m)]^2\, m + 0.11\ [g/(4!m)]^3\, m + O\left(g^4 m^{-3}\right) \ . \tag{6.5}$$

Further details of the perturbative calculation may be found in appendix D.

We now compare the perturbative prediction with results from HT. To do so we extract the mass gap as a function of E_T from truncation calculations for different values of g. Our numerical power limits us to $E_T \leqslant 33m$. At each g we select data in the range $17m < E_T$ and extrapolate this to $E_T \to \infty$ using a fit of the form

$$\mathcal{E}_1 - \mathcal{E}_0 = \alpha_0 + \frac{\alpha_1}{E_T} + \frac{\alpha_2}{E_T} \log\left(\frac{E_T}{m}\right) \ , \tag{6.6}$$

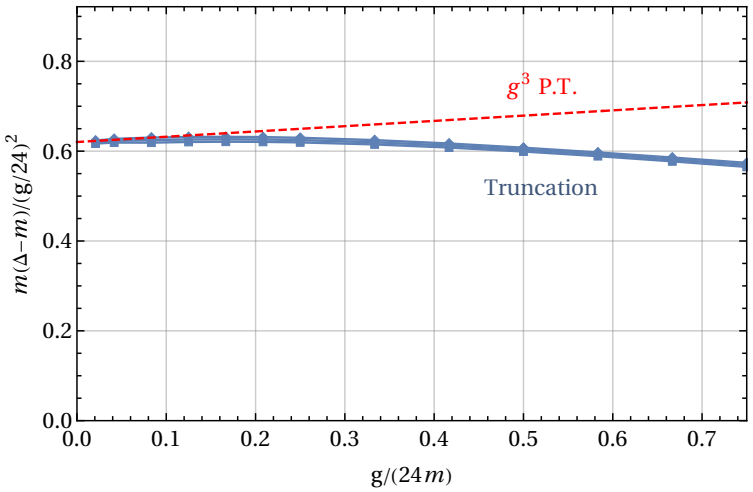


Figure 5: A comparison between the mass gap Δ as a function of g calculated from HT calculations and the perturbative prediction. We plot $m\,(\Delta - m)\,/\,(g/24)^2$ so that the perturbative prediction at $O(g^2)$ is a horizontal line and the $O(g^3)$ prediction is the straight line indicated. Details of the extrapolation of the HT data to $E_T \to \infty$ and the error estimates are given in the main text.

where α_0, α_1 and α_2 are free parameters. This choice of functional form is motivated by naive power counting. Further, in appendix G we show that this form gives precise extrapolations for diagrams at low order in perturbation theory.

We estimate the error σ on the $E_T \to \infty$ extrapolated mass gap $\Delta = \mathcal{E}_1 - \mathcal{E}_0$ by defining

$$\sigma = \max\left(\sigma_{\text{fit}},\ \ |\Delta - \Delta_{\text{high}}|\,,\ \ |\Delta - \Delta_{\text{low}}|\right)\ . \tag{6.7}$$

Here σ_{fit} is the uncertainty on the fit of the full data set with $17m < E_T \leqslant 33m$; Δ_{low} is the extrapolated mass gap obtained when only data up to $E_T = 30m$ is used in the fit, which gives an estimate of the error from our limited numerical power; and Δ_{high} is the extrapolated mass gap obtained when the fit uses only data starting at $E_T = 20m$. Typically the error from the fit is subdominant relative to one of the other uncertainties in (6.7).

The extrapolated results for the mass gap are plotted as a function of g in Figure 5, where the perturbative prediction at order g^3 is also shown. It can be seen that, as expected, the truncation calculation asymptotes to the g^3 prediction as $g \to 0$. The deviation as g increases is consistent with a g^4 correction that has a relatively large coefficient.

As a further test, we have repeated the truncation calculation with different combinations of the counter-terms to cure the primitive divergence and those to add back in missing states missing. In all cases the results obtained do not match the perturbative prediction and appear to be diverging as a function of E_T [albeit slowly for sufficiently small g].

7 Crosscheck through a weak/strong self-duality

In this section we test the numerical power of HT at strong coupling using a weak/strong duality of the ϕ^4 theory, the Magruder duality [27]. We start by deriving the theory and then we present our numerical results.

For the ϕ^4 theory in $d = 2$ spacetime dimensions there is a similar weak/strong duality [28] relating the broken and unbroken phases. The duality has been recently probed using Hamiltonian Truncation [10] and Borel summation [29] techniques. Additionally, ref. [30] studied the strongly coupled phase of ϕ^4 in $[0, T] \times S^2$ manifold and the Magruder duality using Monte Carlo techniques [working in the basis of the $SO(3)$ harmonics, cutting on spin and sampling randomly over the Fock space states].

7.1 Theory

The basic idea is the following, consider the Hamiltonians [22]

$$H = \int_0^L d^2x\, N_m \left(\frac{1}{2}\dot{\phi}^2 + \frac{1}{2}\phi'^2 + \frac{m^2}{2}\phi^2 + g\phi^4 - c(\Lambda, m)\phi^2 \right) + \Omega \tag{7.1}$$

$$H' = \int_0^L d^2x\, N_M \left(\frac{1}{2}\dot{\phi}^2 + \frac{1}{2}\phi'^2 - \frac{M^2}{4}\phi^2 + g\phi^4 - c(\Lambda, M)\phi^2 \right) + \Omega' \tag{7.2}$$

where N_x corresponds to normal ordering with respect to mass x and Ω, Ω' are vacuum counter-terms. [23] The theory is regulated with a momentum cutoff Λ, but other sensible regulators are also possible. The mass counter-term operator is given by

$$c(\Lambda, x) = -\frac{g^2}{6(4\pi)^2} \log \frac{\Lambda}{x}\,, \tag{7.3}$$

The Hamiltonians H and H' act on the infinite dimensional Hilbert space spanned by the free Fock states $|E_i\rangle$ and the counter-terms ensure that the spectrum of both Hamiltonians is finite in the limit $\Lambda \to \infty$. Both theories have the same value for the volume $L \cdot g$. At weak coupling, $g/m \ll 1$ and $g/M \ll 1$, the theory described by H' presents spontaneous symmetry breaking of the $\mathbb{Z}_2$ symmetry, while the theory described by H is in the symmetric phase.

Next we want to relate H to H'. To do so, we need to express the normal-ordered operators in terms of not-normal-ordered ones,

$$N_x(\phi^4) = \phi^4 - 6z_x\phi^2 + 3z_x^2 \;, \qquad N_x(\phi^2) = \phi^2 - z_x \;, \qquad N_x(\dot{\phi}^2 + \phi'^2) = \dot{\phi}^2 + \phi'^2 - y_x\,. \tag{7.4}$$

The functions z_x, y_x are readily computed taking expectation values of the former expressions – leading to $z_m = 1/L \sum_{\vec{k}} \frac{1}{\omega_{\vec{k}}}$ and $y_m = 1/L \sum_{\vec{k}} \frac{2\vec{k}^2 + m^2}{2\omega_{\vec{k}}}$, properly regulated. Then from (7.4), it follows

$$N_m(\phi^4) = N_M(\phi^4) + 6Z_L\phi^2 + v_L \tag{7.5}$$

[22] Originally [27] derived the duality at infinite volume and using a Lagrangian formulation. For our purposes we need to re-derive it in the Hamiltonian description and at finite volume.

[23] We normalise $M^2/4\phi^2$ in order to get M^2 mass-square in the tree-level vacuum.

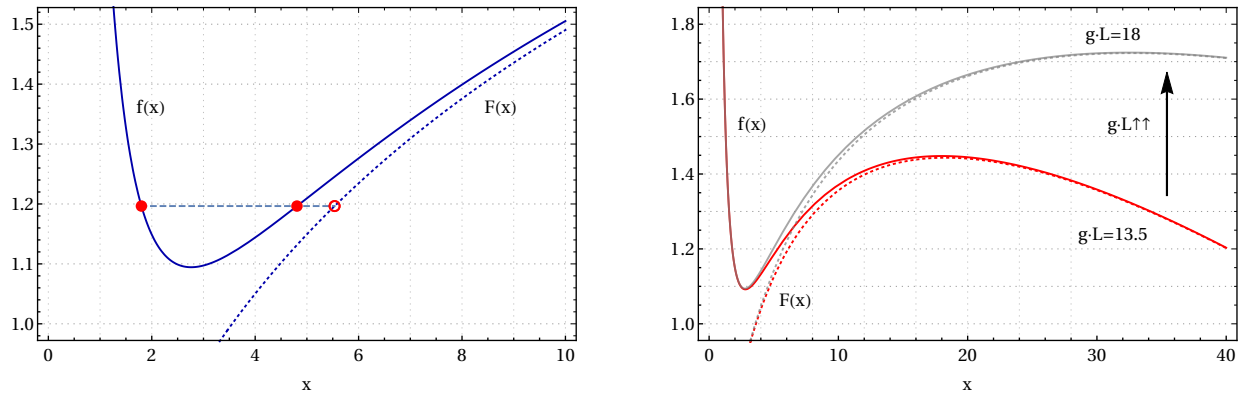


Figure 6: Left: solutions of the duality equation (7.10) are infinite volume. Red dots correspond to two symmetric theories that are dual to each other and to the H' theory signalled with a red circle. Right: solutions of the duality equation (7.10) for $gL \approx \{13.5, 18\}$.

where v_L and Z_L are functions of the volume. We will need

$$Z_L = \sum_{i,j\in\mathbb{Z}} \Delta(L\vec{s}_{ij}; m, M) = \frac{m-M}{4\pi} + \frac{e^{-Lm} - e^{-LM}}{L\pi} + O(e^{-\sqrt{2}Lm}, e^{-\sqrt{2}Lm}) \tag{7.6}$$

where $\Delta(L\vec{s}_{ij}; m, M) \equiv D(L\vec{s}_{ij}; m) - D(L\vec{s}_{ij}; M)$ with $D(\vec{r}; m) = e^{-|r|m}/(4\pi|r|)$, the infinite volume propagator; while the value of v_L is unimportant for our current specific purposes. Using the matching condition (7.5), we find that the two Hamiltonians are equivalent when

$$-\frac{M^2}{4} - g^2 c_2(\Lambda, M) = \frac{m^2}{2} - g^2 c_2(\Lambda, m) + 6gZ_L\,. \tag{7.7}$$

The regulator Λ drops out in the former expression and thus the duality is maintained when the regulator is removed $\Lambda \to \infty$. Let us stress that we have not been careful to match the cosmological constant of both theories, i.e. $\Omega = p(\Omega', z_x, y_x)$. Therefore when (7.7) is satisfied only the mass gap and spectra $\Delta_i \equiv \mathcal{E}_i - \mathcal{E}_0$ of the two theories coincide.

For convenience we define

$$f_{g\cdot L}(x) = \frac{1}{x^2} + \frac{6}{\pi^2}\log x + \frac{3}{\pi x}\left(1 - \frac{4x}{Lg}e^{-Lg/x} + \cdots\right) \tag{7.8}$$

$$F_{g\cdot L}(x) = -\frac{1}{2X^2} + \frac{6}{\pi^2}\log X + \frac{3}{\pi X}\left(1 - \frac{4X}{Lg}e^{-Lg/X} + \cdots\right)\,. \tag{7.9}$$

where $x \equiv \frac{g}{m}$ and $X \equiv \frac{g}{M}$ and $\cdots$ denote further winding modes. Many more winding corrections $[\exp(-Lg/x)]^n$ are easily computed from the definition of Z_L, and in our numerical explorations below we add a large number of winding modes, safely beyond those needed for the values of Lg that we will consider. Now,

$$F_{g\cdot L}(X) = f_{g\cdot L}(x)\,, \tag{7.10}$$

is equivalent to (7.7). The graph of this functions is shown in Figure 6 for various choices of the volume.

Let us discuss the infinite volume limit first, i.e. the left plot of Figure 6. We define $f_\infty \equiv f$ and $F_\infty \equiv F$. The function f has a "V" shape, and for $X \gtrsim 4.43$ [and $L \to \infty$] equation (7.10) has solutions. For $X \gg 1$, the two solutions are $X \approx x$ [following the right branch of f] and $x \approx \pi/\sqrt{6\log(X)}$ [on the left branch]. For the first solution both H and H' are strongly coupled with $x, X \gg 1$; while for the other branch H' at strong coupling is dual to a weakly coupled H theory. Further, the two H theories dual to H' are also dual to each other. For example, the red filled markers in Figure 6 [left plot] indicated the H theories with $x = 1.8$ and $x \approx 4.8$ are equivalent, and both are dual to the H' theory at $X \approx 5.5$, marked with a red circle. Due to the "V" shape of f there is an infinite continuum of pairs of H theories that are self-dual. We will exploit this effect by using relatively large values of f, so that such self-dual pairs are weak/strong dualities. We will do so at finite volume, which we describe next.

In Figure 6 right, we show the graph of $f_{g\cdot L}(x)$ and $F_{g\cdot L}(X)$ for $gL \approx \{13.5, 18\}$. For $gL \gg X, x$ the solutions of (7.7) have a similar two branch "V" shape graph as the infinite volume result. Therefore, when $gL \gg X, x$, the analysis resembles the infinite volume one, and $f_{g\cdot L}$ reaches large enough values that horizontal lines in the right handed plots of Figure 6 cut the solid curve at $x \ll 1$ and $x \gg 1$, showing the existence of weak/strong self-dual H theories. As $gL \gtrsim X, x$ the solutions of (7.7) have a more intricate structure than the infinite volume counterpart duality. In the present work we will not make use of those further strongly coupled theories.

In the next section we are going to exploit the weak/strong self-duality of the H theory to crosscheck our HT results at strong coupling. Namely, we will compute the spectrum of two self-dual theories and check whether compatible results are obtained. Despite the two self-dual Hamiltonians being equivalent it is non-trivial that the two calculations agree. In the more weakly coupled theory the Hamiltonian matrix is close to diagonal. Meanwhile in the more strongly coupled theory there are large off diagonal terms from the ϕ^4 operator and the ϕ^2 counter-term. These off diagonal pieces must combine with the effects of normal ordering and winding corrections to reproduce the dynamics of a weakly coupled theory. Indeed, given that the dimensions of the Hamiltonian are different for the two dual theories at any finite E_T the duality only holds in the $E_T \to \infty$ limit. We are therefore also testing the accuracy of our extrapolations.

In the future it would be interesting to study the duality between a theory with a positive mass squared parameter and one with a negative mass squared parameter. It may also be interesting to compare the vacuum energies or the energies of the higher excited states in the two theories.

7.2 Numerical results

Rather than simply comparing a particular pair of dual theories, we consider the family of theories with $m = 1$ and varying g. As before we fix $L = 4$, and for this value a dual theory exists for any $g \gtrsim 54$. [24] We denote the mass in the dual theory by $\tilde{m}$ and its coupling strength is characterised by $g/\tilde{m}$. The self dual point is at $g = 68.7$. For g smaller than this $\tilde{m} < 1$, so the dual theory is more strongly coupled than the original. For larger g the dual theory is more weakly coupled, and for $g \to \infty$, $\tilde{m} \to \infty$ so the dual theory reaches the perturbative regime. In this limit, the mass

[24] Note that this is a finite volume effect due to the turn over of the right branch in Figure 6 right, and in the infinite volume limit the dual theory exist for any g.

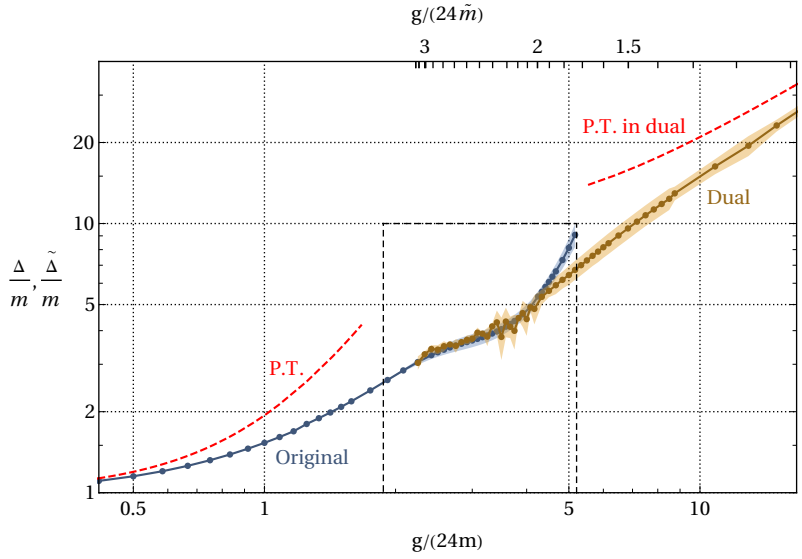


Figure 7: The mass gap in the original [$m = 1$] and dual theories as a function of g, calculated using HT. The strength of the coupling in the dual theory $g/\tilde{m}$ is also indicated. There is a substantial range of couplings where the two calculations agree. The perturbation theory prediction at order g^3 in the original and dual theories is also shown. The same data, zoomed in to the dashed black box, is plotted in Figure 8 left.

gap of the theory can be found by replacing m with $\tilde{m}$ in (6.5).

For each value of g we calculate the mass gap up to the limit of our numerical power $E_T = 33m$. As in section 6, we select data with $E_T > 17m$, and extrapolate to $E_T \to \infty$ with a fit of the form (6.6).[25] We use the same fit form in the dual theories, however the growth of the Fock space with E_T changes with $\tilde{m}$. As a result, we adjust the lower limit on the range of E_T used for the fit, so that data with significant fluctuations is excluded. The maximum accessible $E_T/\tilde{m}$ also changes, and it is largest for the smallest $\tilde{m}$. We estimate the uncertainty on the extrapolated mass gaps as in (6.7).[26]

For very large $\tilde{m}$ it becomes numerically inefficient to carry out the truncation calculation, since $E_T \gg 4\tilde{m}$ cannot be reached. Instead, by dimensional analysis we relate a theory with large $\tilde{m}$ to a theory with $\tilde{m} = 1$ in a box of size $L' = 4\tilde{m}$ with coupling $g/\tilde{m}$. For $L' > 10$ we assume that this theory is close to the infinite volume limit. Its spectrum can be approximated by that of the same theory except with the box size shrunk to $L' = 10$, for which HT is computationally easier. Finally, the results are related back to the large $\tilde{m}$ theory. This trick caps the numerical difficulty as g grows. Choosing the maximum $L' = 10$ it applies to the dual theories with $g \gtrsim 110$.

The results for the extrapolated mass gap in the original and dual theories are plotted as a

[25] Fitting the data with a function $\alpha_0 + \alpha_1/E_T + \alpha_2/E_T^2$, with α_0,α_1,α_2 free parameters leads to results that are sometimes outside the error bars that we quote. However, the CM duality works less well for this choice of extrapolation.

[26] In the dual theory we adjust the definition of Δ_{high} and Δ_{low} to account for the different growth of the basis size with E_T.

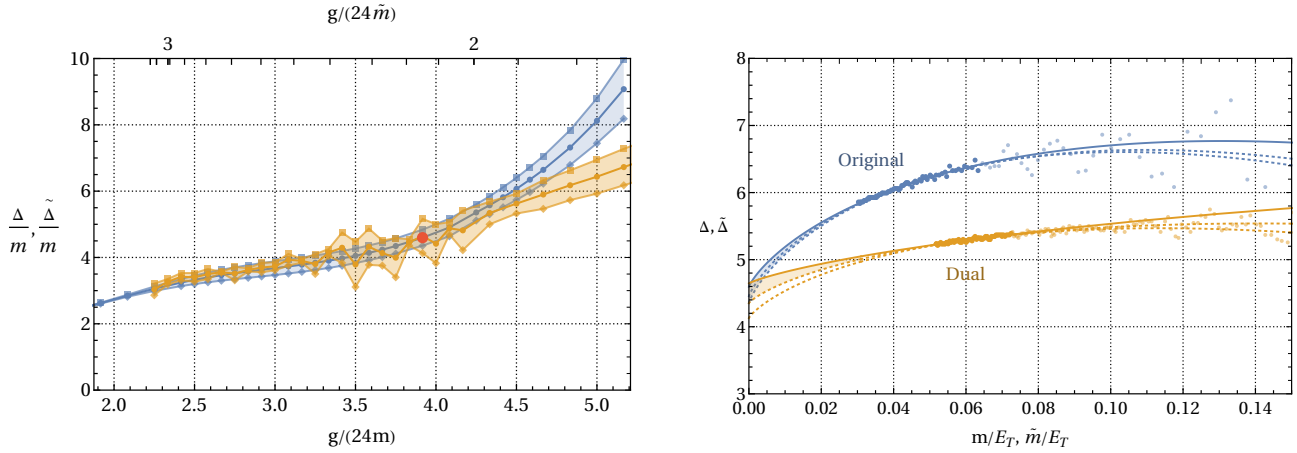


Figure 8: Left: The same data as Figure 7 focusing on the region where the original and dual theories overlap. Right: the results at finite E_T obtained from HT calculations in the original and dual theories for $g = 94$, corresponding to the red dot in the left figure. The extrapolation to $E_T \to \infty$ is also shown, and the data used for this is plotted with solid points. The partially transparent points at small E_T have large fluctuations and are not used for the fit. The extrapolations using data with a smaller maximum E_T or with a larger minimum E_T are plotted with dashed lines. As discussed below (6.7) these are used to estimate the uncertainty on the $E_T \to \infty$ mass gap.

function of g in Figure 7. The same data, shown zoomed in, is plotted in Figure 8 left. When the original theory is weakly coupled enough that it matches the perturbation theory prediction there is no dual theory. In the range from $g = 54$, when the dual theory first exists, up to $g = 100$ there is good agreement between the two theories. For $g > 100$ the dual theory approaches its perturbative prediction, but the original theory deviates. We note that even at $g \simeq 300$ in the dual theory $g/\tilde{m} \simeq 30$ is not tiny. The relative difference between the HT calculation of the mass gap in the dual theory and the perturbative prediction is comparable to the deviation from the perturbative predictions in the original theory at small g/m.

The agreement between the two theories is best, and the uncertainty on the result from the dual theory is smallest, when $g/\tilde{m}$ is largest. This is because $\tilde{m}$ is minimised at this point, and large values of $E_T/\tilde{m}$ can be reached computationally. As a result, the extrapolation to $E_T \to \infty$ is more precise, despite the relatively strong coupling. In the region $g/\tilde{m} \simeq 50$ the results from the dual theory have large uncertainties. Such theories are both strongly coupled and also have a large $\tilde{m}$ so only small values of $E_T/\tilde{m}$ can be accessed. At even larger $g \gtrsim 110$, the trick discussed keeps the maximum accessible $E_T/\tilde{m}$ constant. Since the dual theory becomes gradually more weakly coupled the uncertainty becomes gradually smaller as g increases.

At large g/m the estimated errors on the results from the original theory are not big enough to include the HT results in the dual theory [and at large enough g, the perturbation theory in the dual theory]. This indicates that our approach to estimating the errors breaks down. The reason is that at such large coupling the mass gap is not close to converged for the accessible E_T. Instead are are simply fitting a downward slope, and adjusting the range of the fit does not capture the qualitative change that must happen at E_T beyond our numerical reach.

In Figure 8 right we show the mass gap at finite E_T, and the extrapolation to $E_T \to \infty$, for the original and dual theories at the particular value $g = 94$. The data in the dual theory has less variation with E_T than the original theory, which is expected since the dual is more weakly coupled. However, both are converging toward the same finite value in the large E_T limit. The extrapolations from the reduced data sets that are used to estimate the uncertainties are also plotted.

We note that if this calculation is attempted without including the counterterms to fill in the missing states there is no finite range of g over which the dual theories agree. The deviation of the original theory at $g/m \gtrsim 100$ [in Figure 7] could be a result of our limited numerical reach in E_T. Alternatively, it could be a scheme dependent effect, which we comment on in appendix F.

The agreement between the original and dual theories over a substantial range of g is an encouraging sign for the power of the truncation method. Indeed, the agreement persists until the original theory is fairly strongly coupled with $g/m \simeq 100$ while the dual theory has $g/\tilde{m} \simeq 50$ at this point. It is also interesting that there is a small dip around $g = 90$ in both theories. Preliminary investigation indicates that for larger box sizes this dip may be deeper. This could signal the infinite volume theory having a phase transition to the broken phase at some intermediate coupling.

8 Summary and outlook

In the present work we have analysed Hamiltonian Truncation with UV divergent interactions, focusing our attention on the ϕ^4_3 perturbation in $d = 2 + 1$.

We began by analysing Hamiltonian Perturbation Theory in detail. In particular, we have found that disconnected vacuum diagrams should cancel in an intricate manner but that such cancelation is spoiled if the HT regulator is used, introducing new UV divergences. We proposed a solution that consists of adding back the states that the E_T regulator cuts away, so that all loops are cut at the same energy. Then, we proceeded to formulate HT and we devoted the rest of the paper to inspecting the spectrum of the ϕ^4 theory at weak and strong coupling. We have crosschecked the strongly coupled spectra through a weak/strong self-duality. The strategy and techniques that we have developed will be useful for many other relevant perturbation in $d > 2$ spacetime dimensions.

Given the good quality of our numerical results, we think it is worthwhile to press on and further develop the theory underlying the HT idea. Our *Patch II* may be seen as temporary fix and thus we look forward to more elegant solutions. For instance, a possible avenue consists of introducing an auxiliary momentum cutoff. Namely, consider introducing a momentum cutoff Λ such that $m \ll \Lambda \ll E_T$. When taking the limit $E_T \to \infty$ with Λ kept fixed, the theory is regulated with a single momentum cutoff Λ, all loops are cut equally, and thus many of the problems we discussed associated with the non-covariant regulator are not present. Then, the idea would be to perform the two extrapolations one after the other: $E_T \to \infty$ first and $\Lambda \to \infty$ second. We have done some preliminary study of this idea and it seems computationally challenging, because for each fixed Λ we must reach $E_T \gg \Lambda$.

Next we comment on other directions that we think are worth pursuing.

A key issue for future work will be developing further the theory of improvement terms in $d \geqslant 2+1$. The state of the art analysis is [13]. In our present work, we have shown the power of such improvement terms in $d = 2+1$ in the context of the ϕ^2 perturbation – see e.g. the blue line of Figure 2 left.

It will be fascinating to analyse conformal perturbation theory with a TCSA like cutoff at high order. In view of our results, starting at fourth order the effect of *missing states* should kick in for a vanishing diagonal interaction. Meanwhile for a non-vanishing diagonal interaction, the effect arises at third order. We look forward to developing this in the near future. Interesting work on conformal perturbation theory with a TCSA-like cutoff has been carried out in [17].

Similar comments apply to the Conformal Truncation framework [5]. However, in the light cone, diagrams in which particles are created out of the vacuum are removed [21]. Thus, we expect that in the Conformal Truncation framework some of the problems that we have found will be ameliorated.

A tangential but interesting avenue is the one pursued in [31]. There, precise results for the ϕ^4_2 perturbation were reproduced using Borel series summation techniques. It would be worthwhile to carry out this analysis in $d = 3$ exploiting that the ϕ^4_3 perturbation is Borel summable [for a recent reassessment see [32]], and to compare with our findings. In practice however, this may require a further development on the HT side that we comment on next.

Finally, but not the least, an important aspect that requires a dedicated study is the large volume extrapolation. As the coupling of the $V = g\int^\infty \phi^4$ perturbation is increased, a phase transition where the symmetry $\mathbb{Z}_2 : \phi \to -\phi$ is spontaneously broken can be reached. At the critical point, the theory belongs to the universality class of the 3D Ising model. Therefore, it would be interesting to measure observables of the critical theory using HT. We warn the reader of the *orthogonality catastrophe* of the states as the volume is sent to infinity. Recently such effects have been studied in the HT context for $d = 2$ spacetime [15].

Acknowledgements

We are thankful to Lorenzo Vitale for collaboration at various stages of this project and many useful discussions. We are grateful to Slava Rychkov for initial collaboration, interesting discussions and useful comments on the draft. We acknowledge Matthijs Hogervorst, Marc Montull, Ami Katz, Zuhair Khandker, Marc Riembau, Marco Serone, Giovanni Villadoro and Matthew Walters for interesting discussions and useful comments on the draft.

A Basis of states on a square torus

The symmetry of a square torus is a non-abelian finite group G of $O(2)$. There are 8 elements in this group that can be represented as

$$G = \left\{\mathbb{I}, X, Y, S, S^2, S^3, XS, YS\right\} \tag{A.1}$$

Where S is a rotations by $\frac{\pi}{2}$, X, Y are reflection with respect to horizontal (vertical) axis, and XS, YS are reflections with respect to the diagonals.

The group multiplication table can be compactly summarised by

$$X^2 = \mathbb{I}, \quad S^4 = \mathbb{I}, \quad S^{-1}XS = Y \tag{A.2}$$

The maximal abelian subgroups are $\mathbb{Z}_2 \times \mathbb{Z}_2$ and $\mathbb{Z}_4$,

$$\mathbb{Z}_2 \times \mathbb{Z}_2 : \left\{\mathbb{I}, X, Y, S^2\right\} \tag{A.3}$$

$$\mathbb{Z}_2 \times \mathbb{Z}_2 : \left\{\mathbb{I}, XS, YS, S^2\right\} \tag{A.4}$$

$$\mathbb{Z}_4 : \left\{\mathbb{I}, S, S^2, S^3\right\} \tag{A.5}$$

G is the semidirect product of two abelian subgroups, $G = N \rtimes H$, where N is a normal subgroup (invariant under conjugation). Those can be chosen as

$$N = \mathbb{Z}_4 = \left\{\mathbb{I}, S, S^2, S^3\right\} \tag{A.6}$$

$$H = \mathbb{Z}_2 = \{\mathbb{I}, X\} \tag{A.7}$$

Therefore, the singlets of the full group can be found by choosing states such that $X|\psi\rangle = S|\psi\rangle = |\psi\rangle$. It is likely that the ground state and low energy states are singlets of G, since in perturbation theory the ground states, and the lowest one-particle and two-particles states are all singlets.

The three lowest energy states obtained when diagonalising the complete Fock space are all singlets up these symmetries. The energy of these states can be obtained efficiently by considering a reduced Fock space.

Given the most general non-covariant Fock-space state $|\psi\rangle$, a singlet can be simply constructed as

$$|\psi^S\rangle = \frac{1}{\sqrt{8}}\left(\mathbb{I} + X + Y + S + S^2 + S^3 + X \cdot S + Y \cdot S\right)|\psi\rangle \tag{A.8}$$

However, the normalization is obviously wrong when the Fock-space state is invariant under some (or all) of the symmetries. There are four distinct cases we must consider:

- $|\psi\rangle$ is already invariant under S, but not invariant under X. In that case, the right normalization is
$$|\psi^S\rangle = \frac{1}{\sqrt{2}}\left(\mathbb{I} + X\right)|\psi\rangle \tag{A.9}$$
- $|\psi\rangle$ is only invariant under $A = X, Y, XS, YS$. Then the invariant state is
$$|\psi^S\rangle = \frac{1}{\sqrt{4}}\left(\mathbb{I} + S + S^2 + S^3\right)|\psi\rangle \tag{A.10}$$

- If $|\psi\rangle$ is invariant under both $A = X, Y, XS, YS$ and S^2 then

$$|\psi^S\rangle = \frac{1}{\sqrt{2}} (\mathbb{I} + S) |\psi\rangle \tag{A.11}$$

- If $|\psi\rangle$ is invariant only under S^2 then

$$|\psi^S\rangle = \frac{1}{\sqrt{4}} (\mathbb{I} + X + S + XS) |\psi\rangle \tag{A.12}$$

B Perturbation theory

B.1 Principal equations

In this appendix we give a simple derivation of (3.2). To do so we need to derive an exact effective Hamiltonian. We separate the Hilbert space as $\mathcal{H} = \mathcal{H}_1 \oplus \mathcal{H}_2$. The states are projected as $P_1|y\rangle = |y_1\rangle \in \mathcal{H}_1$ and $(\mathbb{I} - P_1)|y\rangle = |y_2\rangle \in \mathcal{H}_2$. Operators are projected as usual $O_{ij} \equiv P_i O P_j$ with $i, j \in \{1, 2\}$. Then, projecting the eigenvalue equation $H|\mathcal{E}\rangle = \mathcal{E}|\mathcal{E}\rangle$ into the two subspaces we get

$$H_{11}|\mathcal{E}_1\rangle + H_{12}|\mathcal{E}_2\rangle = \mathcal{E}|\mathcal{E}_1\rangle \quad , \qquad H_{21}|\mathcal{E}_1\rangle + H_{22}|\mathcal{E}_2\rangle = \mathcal{E}|\mathcal{E}_2\rangle \, . \tag{B.1}$$

Next we substitute $|\mathcal{E}_2\rangle = (\mathcal{E} - H_{22})^{-1} H_{21}|\mathcal{E}_1\rangle$ from the second equation into the first one and we are led to

$$\left(H_{11} + V_{12} \frac{1}{\mathcal{E} - H_{022} - V_{22}} V_{21} \right) |\mathcal{E}_1\rangle = \mathcal{E} \, |\mathcal{E}_1\rangle \, . \tag{B.2}$$

Now, restricting the $\mathcal{H}_1$ Hilbert space to a single state $|E_i\rangle$, the generalised eigenvalue equation in (B.2) simplifies into the following equation

$$[H_0 + V]_{ii} + V_{ik} [\mathcal{E} - H_0 - V]^{-1}_{kk} V_{ki} - \mathcal{E} = 0 \, , \tag{B.3}$$

where the sum over $k \neq i$ is implicit. [27] All the roots $\mathcal{E}$ of the former equation are the eigenvalues of $H_0 + V$. Then upon plugging in the perturbative ansatz $\mathcal{E}_i = \sum_n g^n \mathcal{E}_i^{(n)}$ in (B.3) and solving for $\mathcal{E}_i^{(n)}$, by consistently equating powers of V, equation (3.2) follows. Thus in general we have the form (3.1), i.e. $\mathcal{E}_i^{(n)} = \langle E_i | \, V([E_i - H_0]^{-1} V)^{n-1} \, |E_i\rangle$ – subtraction terms. For instance, the first few terms read

$$\mathcal{E}_i^{(n)} = \frac{V_{ik_1} V_{k_1 k_2} \cdots V_{k_n i}}{E_{ik_1} E_{ik_2} \cdots E_{ik_{n-1}}} \underbrace{- \mathcal{E}_i^{(2)} \frac{V_{ik_1} V_{k_1 k_2} \cdots V_{k_{n-2} i}}{E_{ik_1} E_{ik_2} \cdots E_{ik_{n-3}}} \sum_{s=1}^{n-3} \frac{1}{E_{ik_s}} - \mathcal{E}_i^{(n-2)} \, V_{ik} E_{ik}^{-2} V_{ki} + \cdots}_{\text{subtraction terms}} \, . \tag{B.4}$$

[27] Note that indices in (B.3) denote matrix elements, while the indices in (B.2) denote the projectors.

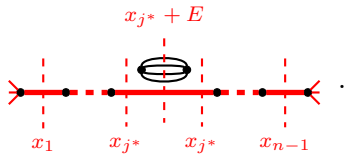
B.2 Cancelation of disconnected two-point bubbles

Next we want to prove a claim that we made in section 5.2.1: namely that disconnected two point bubble diagrams cancel. The proof is based on a recursive argument. First we consider a general nth order diagram contributing to the first term in (B.4). Thus, this diagram can have any external number of lines and can be either connected or disconnected – including possibly containing further two-point bubbles. Next we dress the diagram with a two point bubble in every possible way, i.e. the disconnected two-point bubble spanning from zero to any number of vertices. Finally, we need to show that the sum of all such dressings imply that the two-point bubble factors out and cancels against the second and third term in (B.4). Then, it will follow that no diagrams with disconnected two point bubbles survive after doing the sum of the subtraction terms in (B.4) at any order n.

The dressing of a diagram by a two-point bubble in any possible way is done as follows. First we can dress the diagram by inserting the bubble in between any two consecutive vertices

$$\sum_{j=1}^{n-1} \frac{1}{x_j} \frac{1}{x_j + E} \prod_{i=1}^{n-1} \frac{1}{x_i} \,, \tag{B.5}$$

where $x_0 = x_n = 0$ and where E is the energy propagating in the bubble while x_k is the energy of the other states being propagated in between the vertices. For instance, diagramatically a fixed $j = j^*$ contribution in (B.5) looks like



. (B.6)

Next the two-point buble can span p vertices in all the following possible ways

$$f(p) = \sum_{j=0}^{n-p} \prod_{s=0}^{p} \frac{1}{x_{j+s} + E} \prod_{i=1}^{j} \frac{1}{x_i} \prod_{i=j+p}^{n} \frac{1}{x_i} \,. \tag{B.7}$$

Finally, upon adding $(B.5) + \sum_{p=1}^{n} f(p)$ we are led to

$$\frac{1}{E} \prod_{j=1}^{n-1} \frac{1}{x_j} \sum_{i=1}^{n-1} \frac{1}{x_i} + \prod_{j=1}^{n-1} \frac{1}{x_j} \frac{1}{E^2} \,. \tag{B.8}$$

The former equation has precisely the form of the subtraction terms in (B.4). Indeed, the first term of the former equation should be interpreted as the first term of the *subtraction terms* in (B.4) – with $1/E$ signifying the two-point bubble contribution to $\mathcal{E}_i^{(2)}$ While the second term of the former equation is identified with the second term of the *subtraction terms*. Thus we have established that diagrams containing disconnected two point bubbles do not contribute to $\mathcal{E}_i^{(n)}$. [28] This is of course expected from a covariant Lagrangian calculation, but it is fun to see the intricate way in which it is realised in non-covariant Hamiltonian perturbation theory. Following a similar logic, our proof could be extended to show that all disconnected vacuum diagrams cancel.

[28] Clearly, (B.5) and (B.7) should be multiplied by kinematical factors to get the proper diagrams. But such factors are common to (B.5) and (B.7) and thus they are irrelevant for our main point.

C Calculation of counter-terms

In this appendix we provide details on the calculation of the counter-terms in (5.1) and (5.2). The $O(g^2)$ vacuum diagram is given by

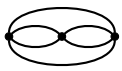


$$= \frac{g^2L^2}{24}\sum \frac{L^2\,\delta_{k_1+k_2+k_3+k_4,0}}{-(\omega_{k_1}+\omega_{k_2}+\omega_{k_3}+\omega_{k_4})}\,, \tag{C.1}$$

were we are using the notation introduced immediately after (3.16). Namely, all the sums include relativistic normalisation, they are performed over all the momenta and are restricted such that the propagating states have energies smaller or equal than E_T. [29] Since the frequencies are restricted to $\omega_{k_1}+\omega_{k_2}+\omega_{k_3}+\omega_{k_4}\leqslant E_T$, we can introduce the factor $1=\int_m^{E_T} dE\delta(E-\Sigma_i\omega_{k_i})$ in the integrand. Then, after switching the order of integration, we are led to $(C.1) = -\frac{g^2L^2}{24}\int_{4m}^{E_T}\frac{dE}{2\pi}\frac{\Phi_4(E)}{E}$, where Φ_4 is the four-particle phase space, given in (3.9). Note that the vacuum energy (C.1) is UV divergent in the limit $E_T\to\infty$. The UV divergence of the vacuum energy density can be evaluated at infinite volume. The infinite volume phase space is given by (3.10). Therefore, we get

$$(C.1) = -(gL)^2\frac{E_T+8m\log\left(m/E_T\right)}{96(4\pi)^3}+O(E_T^0)\,. \tag{C.2}$$

The d_0 counter-term calculation proceeds as follows.



$$= \frac{g^3L^2}{8}\sum \frac{L^2\delta_{k_1+k_2+q_1+q_2,0}}{\omega_{k_1}+\omega_{k_2}+\omega_{q_1}+\omega_{q_2}}\frac{L^2\delta_{k_1+k_2+p_1+p_2,0}}{\omega_{k_1}+\omega_{k_2}+\omega_{p_1}+\omega_{p_2}}\,. \tag{C.3}$$

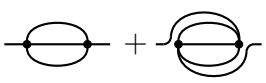
where the symmetry factor is is given by the $m=n=p=2$ of $s^4_{mnp}/4!^3 = 1/[(4-m-n)!(4-m-p)!(4-n-p)!\,m!n!p!]$. Eq. (C.3) leads to a logarithmic UV divergence as $E_T\to\infty$. Different regularisation schemes like momentum cutoff, short distance cutoff or E_T cutoff differ by $O(E_T^0)$. The coefficient of the log divergent piece of (C.3) can be computed at infinite volume [up to the overall extensive L^2 factor] by introducing the phase-space functions Φ_n. In covariant perturbation theory the $O(g^3)$ correction to the vacuum is given by

$$\frac{g^3}{3!\cdot 8}\int_{-\infty}^{\infty}d\tau_1\,d\tau_2\int_{-\infty}^{\infty}d^2y_1d^2y_2\,\Delta^2(\vec{y}_1,\tau_1)\Delta^2(\vec{y}_2,\tau_2)\Delta^2(\vec{y}_1+\vec{y}_2,\tau_1+\tau_2)\,. \tag{C.4}$$

The former expression can be written as $(C.4) = \frac{g^3}{8}\int_{-\infty}^{\infty}\frac{d^3k}{(2\pi)^3}\,\rho^3(k)$ where we have defined $\rho(k) = \frac{1}{3!}\int_{-\infty}^{\infty}d\tau\int_{-\infty}^{\infty}\Delta^2(z)e^{i\mathbf{k}\cdot\vec{z}}d^2z$. Given $\Delta(z)=e^{-m|z|}/(4\pi|z|)$, we get $\rho(k)=\frac{1}{3!}\frac{1}{8k}+\cdots$. Therefore, [30]

$$(C.3) = \frac{1}{3!}\frac{g^3L^2}{2^9\,(4\pi)^2}\log(E_T/m)+O(E_T^0)\,. \tag{C.5}$$

Finally, the mass gap $\mathcal{E}_1^{(2)}-\mathcal{E}_0^{(2)}$ at $O(g^2)$ is given by



$$= \frac{g^2}{12m}\sum\frac{L^2\delta_{k_1+k_2+k_3,0}}{1-(\omega_{k_1}+\omega_{k_2}+\omega_{k_3})}+\frac{L^2\delta_{k_1+k_2+k_3,0}}{1-(\omega_{k_1}+\omega_{k_2}+\omega_{k_3}+2)}\,, \tag{C.6}$$

[29] In the case at hand the notation means $\sum=\sum_{k_i\ \text{s.t.}\ E_{\rm in}\leqslant E_T}1/\prod_j 2L^2\omega_{k_j}$ where $E_{\rm in}=\omega_{k_1}+\omega_{k_2}+\omega_{k_3}+\omega_{k_4}$.

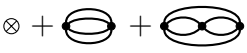
[30] This result agrees with dimensional regularisation or momentum cutoff regularisation, which can be found elsewhere in the literature, see for instance Eq. (C7) of ref. [33].

where, as drawn in the former two diagrams, we need to take into account that there are two possible vertex orderings. Again, we can evaluate the UV divergence of the former expression by introducing the phase space Φ_3 at infinite volume. Then, in the limit $m \ll E_T$ we get

$$(C.6) = \Big(-\frac{g^2}{96\pi^2}\log(E_T/m) + O(E_T^0)\Big) \cdot \langle m|V_2|m\rangle \,. \tag{C.7}$$

D Perturbative mass

In this appendix we give details on the computation of the mass gap and vacuum energy in Hamiltonian perturbation theory with the E_T regulator. We do the calculation up to $O(g^3)$. Note that $V_{nn} \times V_{nk}(E_n - E_k)^{-2}V_{kn} = O(g^4)$, since the only non-vanishing terms are $\langle n|C|n\rangle = O(g^2)$. Thus we are left to compute the zero, one, two and three point functions. The vacuum and first excited states are given by

$\mathcal{E}_0(E_T)$ =  (D.1)

$\mathcal{E}_1(E_T)$ = 

 (D.2)

Where the diagrams are given by the following expressions:

 $= -\frac{g^2}{24}\sum \frac{1}{\prod_{j=1}^4 2L^2\omega_{\vec{k}_j}} \frac{L^2\delta_{k_1+k_2+k_3+k_4,0}}{\omega_{k_1}+\omega_{k_2}+\omega_{k_3}+\omega_{k_4}} \cdot L^2 \,,$ (D.3)

 $= \frac{g^3}{8}\sum \frac{L^2\delta_{k_1+k_2+q_1+q_2,0}}{\omega_{k_1}+\omega_{k_2}+\omega_{q_1}+\omega_{q_2}} \frac{L^2\delta_{k_1+k_2+p_1+p_2,0}}{\omega_{k_1}+\omega_{k_2}+\omega_{p_1}+\omega_{p_2}} \cdot L^2 \,,$ (D.4)

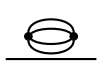
 $= m \,,$ (D.5)

 $= -c_2 \cdot \langle m|V_2|m\rangle \,,$ (D.6)

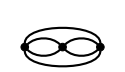
 $= -(c_0+d_0)\cdot L^2 \,,$ (D.7)

 $= -\frac{g^2}{6}\sum \frac{L^2\delta_{k_1+k_2+k_3,0}}{-m+\omega_{k_1}+\omega_{k_2}+\omega_{k_3}} \cdot \langle m|V_2|m\rangle \,,$ (D.8)

 $= -\frac{g^2}{6}\sum \frac{L^2\delta_{k_1+k_2+k_3,0}}{m+\omega_{k_1}+\omega_{k_2}+\omega_{k_3}} \cdot \langle m|V_2|m\rangle \,,$ (D.9)

 $= -\frac{g^2}{24}\sum \frac{L^2\delta_{k_1+k_2+k_3+k_4,0}}{\omega_{k_1}+\omega_{k_2}+\omega_{k_3}+\omega_{k_4}} \cdot L^2 \,,$ (D.10)

 $= \frac{gc_2}{4}\sum \frac{L^2\delta_{k_1+k_2,0}}{\omega_{k_1}+\omega_{k_2}} \cdot 2\langle m|V_2|m\rangle \,,$ (D.11)

 $= \frac{g^3}{8}\sum \frac{L^2\delta_{k_1+k_2+q_1+q_2,0}}{\omega_{k_1}+\omega_{k_2}+\omega_{q_1}+\omega_{q_2}} \frac{L^2\delta_{k_1+k_2+p_1+p_2,0}}{\omega_{k_1}+\omega_{k_2}+\omega_{p_1}+\omega_{p_2}} \cdot L^2 \,,$ (D.12)

 $= \frac{g^3}{4}\sum \frac{L^2\delta_{\vec{p}_1+\vec{p}_2+\vec{k},0}}{-m+\omega_{p_1}+\omega_{p_2}+\omega_k} \frac{L^2\delta_{\vec{q}_1+\vec{q}_2+\vec{k},0}}{-m+\omega_{q_1}+\omega_{q_2}+\omega_k} \cdot \langle m|V_2|m\rangle \,,$ (D.13)



$$= \frac{g^3}{4}\sum \frac{L^2\delta_{\vec{p}_1+\vec{p}_2+\vec{k},0}}{m+\omega_{p_1}+\omega_{p_2}+\omega_k}\frac{L^2\delta_{\vec{q}_1+\vec{q}_2+\vec{k},0}}{m+\omega_{q_1}+\omega_{q_2}+\omega_k}\cdot\langle m|V_2|m\rangle\,, \tag{D.14}$$



$$= \frac{g^3}{4}\sum \frac{L^2\delta_{p_1+p_2+p_3,0}}{m+\omega_{p_1}+\omega_{p_2}+\omega_{p_3}}\frac{L^2\delta_{q_1+q_2+p_1+p_2,0}}{\omega_{q_1}+\omega_{q_2}+\omega_{p_1}+\omega_{p_2}}\cdot\langle m|V_2|m\rangle\,, \tag{D.15}$$



$$= \frac{g^3}{4}\sum \frac{L^2\delta_{p_1+p_2+p_3,0}}{-m+\omega_{p_1}+\omega_{p_2}+\omega_{p_3}}\frac{L^2\delta_{q_1+q_2+p_1+p_2,0}}{\omega_{q_1}+\omega_{q_2}+\omega_{p_1}+\omega_{p_2}}\cdot\langle m|V_2|m\rangle\,, \tag{D.16}$$



$$= \frac{g^3}{12}\sum \frac{L^2\delta_{p_1+p_2+p_3+p_4,0}}{\omega_{p_1}+\omega_{p_2}+\omega_{p_3}+\omega_{p_4}}\frac{L^2\delta_{q+p_1,0}}{\omega_{p_1}+\omega_q}\cdot 2\langle m|V_2|m\rangle\,, \tag{D.17}$$



$$= \frac{g^3}{12}\sum \frac{L^2\delta_{k_1+k_2+k_3+p,0}}{\omega_{k_1}+\omega_{k_2}+\omega_{k_3}+\omega_p}\cdot\frac{L^2\delta_{k_1+k_2+k_3+q,0}}{\omega_{k_1}+\omega_{k_2}+\omega_{k_3}+\omega_q}\cdot 2\langle m|V_2|m\rangle\,. \tag{D.18}$$

The sums in the previous expressions are over all momenta and involve relativistic measures, namely

$$\sum \equiv \sum_{\substack{\text{all } k_i \\ \text{s.t. } E_{\text{in}}\leqslant E_T}} \frac{1}{2L^2\omega_{k_i}}\,, \tag{D.19}$$

where E_{in} is the energy of the sate propagating between any to given consecutive vertices. Many of this expression can be computed analytically while other can be easily evaluated numerically with your favourite package. We used `vegas`, a `python` package that implements Monte Carlo integration. Combined, the results lead to equation (6.5) in the main text.

Note that the diagrams in (D.17) are logarithmically UV divergent. Indeed, in the limit $E_T \sim k_i \gg q, p \sim m$, they combine into

$$(D.17) = \frac{g^3}{6}\sum \frac{L^2\delta_{q+p,0}}{\omega_p+\omega_q}\sum \frac{L^2\delta_{k_1+k_2+k_3+p,0}}{\omega_{k_1}+\omega_{k_2}+\omega_{k_3}+\omega_p} + O(1/E_T) = -\frac{gc_2}{4}\sum \frac{L^2\delta_{q+p,0}}{\omega_p+\omega_q} + O(1/E_T)\,,$$

and, unsurprisingly the UV divergence cancels against diagram (D.11).

E Algorithmic implementation

Our implementation of the truncation calculation largely follows that described in [15], with some additional complications due to having one extra dimension and from the counter-terms needed to patch up for missing states.

We first construct a basis of all states with momenta purely in the first quadrant. A zero momentum state is then represented in terms of these states rotated into each of the quadrants [along with zero momentum quanta]. When computing the Hamiltonian matrix, the vast majority of the overlaps between states vanish, i.e. the matrix is extremely sparse. The key algorithmic requirement is that excessive time is not spent computing matrix elements that turn out to be zero. To avoid this we initially compute the states that can be produced from each basis element when $n = 1, 2, 3, 4$ creation or annihilation operators applied. The results of this are stored as maps [or dictionaries] with the momentum change as the keys. Many of the numerical quantities involved in the matrix elements can also be computed in advance and stored in maps. Used together these

allow only non-zero matrix elements to be computed, and such computations amount to simply multiplying a handful of previously saved numbers.

The counter-terms that correct for missing states can be straightforwardly calculated in the code. We replace integrals with sums over states so that finite volume corrections are captured. Then the counterterm fixing a single two-point bubble with vertices consecutive in time, (5.38), is given by

$$\delta V^I_{nn} = \sum_4 \frac{V_{04}V_{40}}{E_{i(n+4)}} \,, \tag{E.1}$$

where 4 represents a 4-particle state, and the sum is restricted to states such that $E_T - E_n < E_4 \leqslant E_T$. The counterm corresponding to towers of overlapping two-point bubbles can be calculated via matrix products. For example, the part of (5.44) that corresponds to two iterated bubbles is given by

$$\delta V^{II}_{nn} \supset \sum_{4,4'} \frac{V_{04}V_{4(4+4')}V_{(4+4')4'}V_{4'0}}{E_{i(n+4)}E_{i(n+4+4')}E_{i(n+4')}} \,, \tag{E.2}$$

where 4 and $4'$ represent the four particle states that make up to the two bubbles. The sum is restricted to 4 and $4'$ such that at least one of $E_4 > E_T - E_n$ and $E_{4'} > E_T - E_n$ is satisfied.[31]

In our numerical calculations we also include a counterterm δV^{III}_{nn} that accounts for the missing states in the three-point vacuum bubble diagram. This is not needed for a UV finite theory, and in practice only leads to extremely minor change to the numerical results, but it does slightly simplify the Monte Carlo integration in section G. We have checked and find that adding further corrections to account for other classes of missing states [scaling either as E_T^0 or as $1/E_T^n$ with $n > 1$] also does not significantly change the numerical results that we show in section 6 and 7.

Efficient algorithms for finding the smallest few eigenvalues of sparse matrices are well known, and we simply use the library Eigen. In our implementation the majority of the computational time is spent obtaining the eigenvalues themselves from the Hamiltonian matrix, although calculating the state dependent counter-term corresponding to the towers of vacuum bubbles is also expensive. On a personal computer we reach basis sizes of order 10^6, and using a single node of a high performance cluster we are limited to basis sizes $\lesssim 10^7$. At the maximum basis size the lowest eigenvalues can be computed in approximately an hour. We are unable to access larger basis sizes due to memory limitations on the size of the Hamiltonian matrix itself [despite being stored in sparse form].

F Finite mismatch pieces

In the main text we focused on, and corrected for, new UV divergences due to an E_T regulator. In this appendix, we consider effects introduced by such a regulator that remain finite as $E_T \to \infty$. First in appendix F.1 we identify the types of diagram that lead to such corrections. Then, in

[31] The counterterms δV^I_{nn} and δV^{II}_{nn} are computationally expensive to implement since they must be calculated for each energy E_n individually. In practice we compute the counter-terms once for state energies $E_n = 0, m/10, 2m/10, \ldots, E_T$ and store the results. Then when inserting the counterterms into the matrix, for a state E_n we simply use the nearest saved value. We have checked this makes no difference to the numerical results.

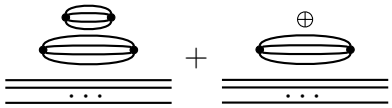
appendix F.2 we argue that the weak/strong duality tests how important such finite corrections are for our numerical results from HT.

F.1 Sources of finite regulator dependence

The sources of finite corrections can be identified by continuing the analysis in section 5.2. Only diagrams with at least one UV divergent sub-diagram can be sensitive to the regulator, so the possibilities are limited.

All classes of diagrams analysed in 5.3 that give extra UV divergent pieces also give finite corrections. Our patches in section 5.3 account for the missing states in the divergent parts of such diagrams, for example the upper bubble of (5.23). So there is no finite correction from the E_T regulator on this loop.

However, there can be finite corrections from the other, unpatched, loops, e.g. the lower bubble in (5.23). This can be seen by considering a simplified version of the diagram with just an state of energy x_s below



(F.1)

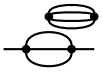
where the second diagram corresponds to the counter-term adding back in states to the upper bubble. Regulating the lower loop by $E_T - X_s$

$$(\text{F.1}) = -\text{sym} \int_4^{E_T - X_s} dx_1 \frac{\Phi_4(x_1)}{x_1^2} \int_4^{E_T} dx_2 \frac{\Phi_4(x_1)}{x_1 + x_2} \,, \tag{F.2}$$

where sym is the symmetry factor, and x_1 and x_2 are the energies in the lower and upper bubbles, and the x_2 integral extends to E_T due to the patch up. Carrying out the integrals and expanding at large E_T we find a finite sensitivity to X_s. On the other hand, there is no finite piece from the un-patched sunset bubble in (5.22), due to the faster convergence of the lower loop in this case.

There are also diagrams that do not result in UV divergent contributions but do give finite pieces. For example, this happens when a two-point vacuum bubble with its vertices consecutive in time is inserted above a convergent diagram. Indeed, we have already seen this in (5.29). Such diagrams are automatically fixed by (5.38). Meanwhile in (5.31) the sunset diagram and the three-point vacuum bubble do not give such finite pieces.

Finite pieces also arise when the two-point vacuum bubble crosses one of the vertices of a logarithmically divergent diagram. For example,

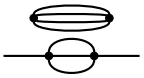


(F.3)

gives $g_{E_i}(x_s) \sim x_s^0$ in (5.26) [where x_s is the energy in the sunset loop]. Extracting the part of (F.3) that depends on X_s, and setting $X_s = x_s$, the finite correction is evident. Further, a tower of two point bubbles crossing a vertex of the sunset diagram gives a similar correction. The same happens when a two-point bubble, or a tower of these, crosses one of the vertices of the vacuum

three-point bubble [calculating the correction analogously to (5.25), we see that this could either be one of the outer vertices or the central one]. Such effects are not corrected by our patches.

Finally, finite pieces are produced when a sunset diagram has both vertices spanned by a two-point vacuum bubble,



(F.4)

given by

$$(F.4) = -\text{sym} \int_4^{E_T} dx_4 \frac{\Phi_4(x_4)}{x_4^2} \int_3^{E_T - X_4} dx_3 \frac{\Phi_3(x_3)}{(x_3 + x_4)} \ , \tag{F.5}$$

where x_3 and x_4 are the energies in the sunset and two-point bubble respectively. Then the dependence on the regulator can be extracted from the leading term proportional to X_4. Dropping order 1 factors for clarity, this scales as

$$\sim \int_4^{E_T} dx_4 \frac{\Phi_4(x_4)}{x_4^2} \left(\frac{X_4}{E_T} \right) \ , \tag{F.6}$$

so after setting $x_4 = X_4$ a finite piece remains.[32]

Carrying out a similar analysis for the subtraction terms shows that these also generate extra finite pieces $O(E_T^0)$ that are sensitive to the E_T cutoff regulator.

Although finite corrections in themselves do not prevent the theory being well defined as $E_T \to \infty$, it might be wondered what happens once they are embedded in more complex diagrams. We have checked these effects in diagrams of up to $O(g^8)$ and we have not identified any such structures in the perturbation theory that are dangerous. An all orders proof and general understanding of this would be very desirable in the future.

F.2 Finite pieces and the weak/strong self-duality

As mentioned in section 7, as well as testing the numerical power of HT, the weak strong duality plays a second important role: it tests how large the effect of finite corrections due to the E_T regulator is. The duality does so because the regulator dependent corrections to the mass gap of a theory depends on the particle's unperturbed mass. Consequently, the values of the finite corrections will differ between the original and dual theories.

For example, consider the diagram (F.1) but with the state below the bubbles simply a single particle state. Then the lower bubble is cut by $E_T - X_s$ where due to the E_T regulator X_s. Once the corresponding integrals are evaluated and the X_s dependence is extracted, it can be seen that the finite correction is proportional to the particle's unperturbed mass.

Since we find that the original and dual theories give results that agree well over an extended range of couplings, we conclude that finite pieces are not playing a major role. Consequently, at least up to $g \simeq 100$, we are working in a scheme that could be reproduced in a calculation with a covariant regulator to reasonable accuracy.

[32] An analogous calculation shows that a two-point vacuum bubble spanning two, or all three, of the vertices of a three-point vacuum bubble does not give a finite contribution.

G Monte Carlo integration of low order diagrams

In this appendix we evaluate diagrams at low order in perturbation theory in ϕ^4 in 2+1 dimensions using Monte Carlo integration. By doing so we confirm that HT results at relatively small E_T can be accurately extrapolated to the $E_T \to \infty$ limit. We also find that form (6.5) leads to a more precise extrapolation than possible alternative choices.

In the Monte Carlo integrals we implement exactly the same E_T cutoff as occurs in a truncation calculation, and we study the dependence of the diagrams on E_T. Unlike truncation calculations, Monte Carlo integration can reach large values of E_T, although each diagram must be calculated individually.[33] The counter-terms to remove the primitive divergences, and to add back in missing states in these integrations, are taken to be identical to those that we use in truncation calculations.

The diagrams that contribute to the mass gap at order g^2 and g^3 are given in equations (6.1),(6.2), (6.3) and (6.4). Although not necessary to obtain a finite UV theory, we add back in the contribution from the missing states to the disconnected 3-point bubble. As a result such a diagram cancels between $\mathcal{E}_1^{(3)}$ and $\mathcal{E}_0^{(3)}$ in the calculation of the mass gap at finite E_T as well as in the large E_T limit.

We calculate all of the preceding diagrams with Monte Carlo integration for a box length $L = 4/m$. The results are shown as a function of E_T in Figure 9. The prediction for the mass gap in the limit $E_T \to \infty$, (6.5), is obtained by extrapolating the data including all values of E_T. The Monte Carlo results obtained are relatively smooth once E_T is not too small, which is compatible with the HT results shown in Figure 4.

To test the potential power of the truncation method, we select only those Monte Carlo data points that can be reached in our truncation code. For $L = 4/m$ this corresponds to those with $E_T < 34m$. We also exclude points with $E_T < 17m$ since these have large fluctuations. We fit such data points with a function of the form of (6.6). The results of these fits and their extrapolation to large E_T are shown in Figure 9.

At the values of E_T that are accessible in truncation calculations the g^2 correction reaches within 5% of its asymptotic value. The extrapolation of this to $E_T \to \infty$ gives a prediction that coincides with the full result to better than 0.1% accuracy. In contrast, at the accessible E_T the g^3 correction is not only far from its asymptotic value but even of opposite sign. Despite this, the extrapolation of the g^3 correction from the small E_T data matches that of the full data set to within 3%. The results obtained for the vacuum energy are qualitatively and quantitatively similar. For both the mass gap and the vacuum energy calculations, we find that the functional form (6.6) gives a more accurate extrapolation than if the α_2 part is excluded, or if this is replaced by a piece α_2/E_T^2.

As discussed in section 6, we estimate the coupling g^* above which the theory is strongly coupled by demanding that $\mathcal{E}_0^{(3)} = \mathcal{E}_0^{(2)}$ at this value, which gives $g^* = 8.3$. The g^3 correction to the mass gap is suppressed relative to the g^2 correction at this value. However, most of this suppression is due to an accidental (one in four) cancellation between convergent subsets of diagrams. Taking each convergent subset individually, our estimate of strong coupling based on the mass gap would

[33] We use the python package Vegas for our Monte Carlo results.

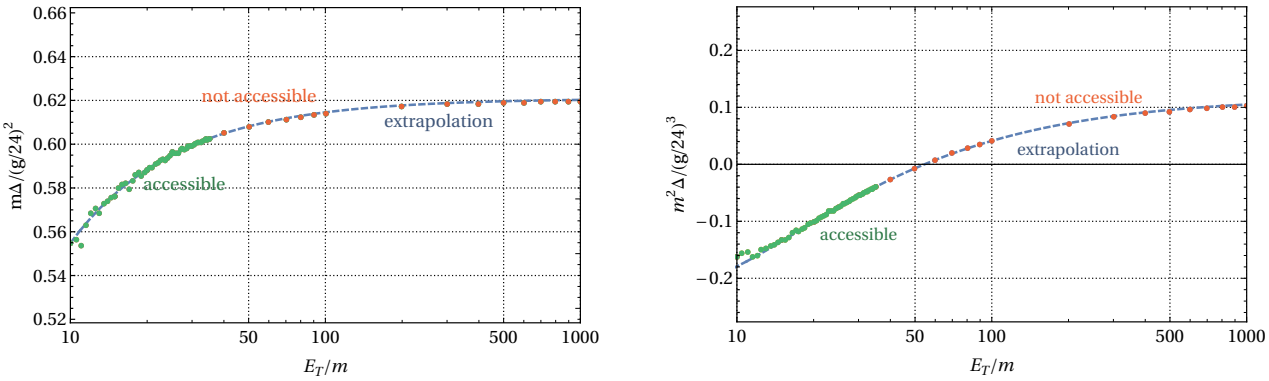


Figure 9: Data from Monte Carlo integration of perturbation theory diagrams showing the convergence of the g^2 (left) and g^3 (right) corrections to the mass gap $\Delta = \mathcal{E}_1 - \mathcal{E}_0$ as a function of the energy cutoff E_T in ϕ^4 theory in $2+1$ dimensions for a box size $L = 4/m$. We indicate values of E_T that are accessible and not accessible in HT calculations, and the extrapolation of the former.

be $g^* \sim 30$.

Unlike Monte Carlo integration of diagrams, a truncation calculation is not perturbative in g. Nevertheless, the Monte Carlo data is a positive indication that precise numerical results can be obtained from truncation calculations.

References

[1] V. P. Yurov and A. B. Zamolodchikov, "Truncated Conformal Space Approach to scaling Lee-Yang Model," *Int. J. Mod. Phys.* **A5** (1990) 3221–3246.

[2] V. P. Yurov and A. B. Zamolodchikov, "Truncated fermionic space approach to the critical 2-D Ising model with magnetic field," *Int. J. Mod. Phys.* **A6** (1991) 4557–4578.

[3] E. Katz, G. Marques Tavares, and Y. Xu, "A solution of 2D QCD at Finite N using a conformal basis," arXiv:1405.6727 [hep-th].

[4] E. Katz, G. Marques Tavares, and Y. Xu, "Solving 2D QCD with an adjoint fermion analytically," *JHEP* **05** (2014) 143, arXiv:1308.4980 [hep-th].

[5] E. Katz, Z. U. Khandker, and M. T. Walters, "A Conformal Truncation Framework for Infinite-Volume Dynamics," *JHEP* **07** (2016) 140, arXiv:1604.01766 [hep-th].

[6] A. L. Fitzpatrick, J. Kaplan, E. Katz, L. G. Vitale, and M. T. Walters, "Lightcone effective Hamiltonians and RG flows," *JHEP* **08** (2018) 120, arXiv:1803.10793 [hep-th].

[7] L. V. Delacretaz, A. L. Fitzpatrick, E. Katz, and L. G. Vitale, "Conformal Truncation of Chern-Simons Theory at Large N_f," *JHEP* **03** (2019) 107, arXiv:1811.10612 [hep-th].

[8] E. D. Brooks, III and S. C. Frautschi, "Scalars Coupled to Fermions in (1+1)-dimensions," *Z. Phys.* **C23** (1984) 263.

[9] S. Rychkov and L. G. Vitale, "Hamiltonian truncation study of the ϕ^4 theory in two dimensions," *Phys. Rev.* **D91** (2015) 085011, arXiv:1412.3460 [hep-th].

[10] S. Rychkov and L. G. Vitale, "Hamiltonian truncation study of the ϕ^4 theory in two dimensions. II. The $\mathbb{Z}_2$ -broken phase and the Chang duality," *Phys. Rev.* **D93** no. 6, (2016) 065014, arXiv:1512.00493 [hep-th].

[11] J. Elias-Miro, M. Montull, and M. Riembau, "The renormalized Hamiltonian truncation method in the large E_T expansion," *JHEP* **04** (2016) 144, arXiv:1512.05746 [hep-th].

[12] Z. Bajnok and M. Lajer, "Truncated Hilbert space approach to the 2d ϕ^4 theory," *JHEP* **10** (2016) 050, arXiv:1512.06901 [hep-th].

[13] J. Elias-Miro, S. Rychkov, and L. G. Vitale, "High-Precision Calculations in Strongly Coupled Quantum Field Theory with Next-to-Leading-Order Renormalized Hamiltonian Truncation," arXiv:1706.06121 [hep-th].

[14] A. J. A. James, R. M. Konik, P. Lecheminant, N. J. Robinson, and A. M. Tsvelik, "Non-perturbative methodologies for low-dimensional strongly-correlated systems: From non-abelian bosonization to truncated spectrum methods," *Rept. Prog. Phys.* **81** no. 4, (2018) 046002, arXiv:1703.08421 [cond-mat.str-el].

[15] J. Elias-Miro, S. Rychkov, and L. G. Vitale, "NLO Renormalization in the Hamiltonian Truncation," *Phys. Rev.* **D96** no. 6, (2017) 065024, arXiv:1706.09929 [hep-th].

[16] M. Hogervorst, S. Rychkov, and B. C. van Rees, "Truncated conformal space approach in d dimensions: A cheap alternative to lattice field theory?," *Phys. Rev.* **D91** (2015) 025005, arXiv:1409.1581 [hep-th].

[17] D. Rutter and B. C. van Rees, "Counterterms in Truncated Conformal Perturbation Theory," arXiv:1803.05798 [hep-th].

[18] N. Anand, Z. U. Khandker, and M. T. Walters, "Momentum space CFT correlators for Hamiltonian truncation," arXiv:1911.02573 [hep-th].

[19] M. Hogervorst, "RG flows on S^d and Hamiltonian truncation," arXiv:1811.00528 [hep-th].

[20] S. Groote, J. G. Korner, and A. A. Pivovarov, "On the evaluation of sunset - type Feynman diagrams," *Nucl. Phys.* **B542** (1999) 515–547, arXiv:hep-ph/9806402 [hep-ph].

[21] S. Weinberg, "Dynamics at infinite momentum," *Phys. Rev.* **150** (1966) 1313–1318.

[22] S. R. Coleman and E. J. Weinberg, "Radiative Corrections as the Origin of Spontaneous Symmetry Breaking," *Phys. Rev.* **D7** (1973) 1888–1910.

[23] G. Feverati, K. Graham, P. A. Pearce, G. Z. Toth, and G. Watts, "A Renormalisation group for TCSA," *J. Stat. Mech.* (2008) P03011, arXiv:hep-th/0612203 [hep-th].

[24] G. M. Watts, "On the renormalisation group for the boundary Truncated Conformal Space Approach," *Nucl.Phys.* **B859** (2012) 177–206, arXiv:1104.0225 [hep-th].

[25] M. Lencses and G. Takacs, "Excited state TBA and renormalized TCSA in the scaling Potts model," *JHEP* **09** (2014) 052, arXiv:1405.3157 [hep-th].

[26] S. Weinberg, *The quantum theory of fields. Vol. 2: Modern applications*. Cambridge University Press, 2013.

[27] S. F. Magruder, "The Existence of Phase Transition in the (phi**4) in Three-Dimensions Quantum Field Theory," *Phys. Rev.* **D14** (1976) 1602.

[28] S.-J. Chang, "The Existence of a Second Order Phase Transition in the Two-Dimensional ϕ^4 Field Theory," *Phys.Rev.* **D13** (1976) 2778.

[29] M. Serone, G. Spada, and G. Villadoro, "$\lambda\phi^4_2$ theory ? Part II. the broken phase beyond NNNN(NNNN)LO," *JHEP* **05** (2019) 047, arXiv:1901.05023 [hep-th].

[30] M. Windoloski, "A Nonperturbative study of three-dimensional phi**4 theory," arXiv:hep-th/0002243 [hep-th].

[31] M. Serone, G. Spada, and G. Villadoro, "$\lambda\phi^4$ Theory I: The Symmetric Phase Beyond NNNNNNNNLO," *JHEP* **08** (2018) 148, arXiv:1805.05882 [hep-th].

[32] G. Sberveglieri, M. Serone, and G. Spada, "Renormalization scheme dependence, RG flow, and Borel summability in ϕ^4 Theories in $d < 4$," *Phys. Rev.* **D100** no. 4, (2019) 045008, arXiv:1905.02122 [hep-th].

[33] E. Braaten and A. Nieto, "Effective field theory approach to high temperature thermodynamics," *Phys. Rev.* **D51** (1995) 6990–7006, arXiv:hep-ph/9501375 [hep-ph].